PROCEEDINGS OF SPIE

MYSTIC: a high angular resolution K-band imager at CHARA

Benjamin Setterholm, John Monnier, Jean-Baptiste Le Bouquin, Narsireddy Anugu, Jacob Ennis, et al.

SPIE.

MYSTIC: a high angular resolution K-band imager at CHARA

Benjamin R. Setterholm[a], John D. Monnier[a], Jean-Baptiste Le Bouquin[b], Narsireddy Anugu[c], Jacob Ennis[a], Becky Flores[d], Tyler Gardner[a], Nour Ibrahim[a], Laurent Jocou[b], Stefan Kraus[e], Cyprien Lanthermann[c], Gail Schaefer[c], and Theo ten Brummelaar[c]

[a]University of Michigan, Department of Astronomy, 1085 S. University, Ann Arbor, MI 48109, USA
[b]Institut de Planétologie et d'Astrophysique de Grenoble, Grenoble F-38058, France
[c]The CHARA Array of Georgia State University, Mount Wilson Observatory, Mount Wilson, CA 91203, USA
[d]Georgia State University, Department of Physics and Astronomy, Atlanta, GA 30302, USA
[e]University of Exeter, Department of Physics & Astronomy, Stocker Road, Exeter EX4 4QL, UK

ABSTRACT

The Michigan Young STar Imager at CHARA (MYSTIC) is a K-band interferometric beam combining instrument funded by the United States National Science Foundation, designed primarily for imaging sub-au scale disk structures around nearby young stars and to probe the planet formation process. Installed at the CHARA array in July 2021, with baselines up to 331 meters, MYSTIC provides a maximum angular resolution of $\lambda/2B \sim 0.7$ mas. The instrument injects phase corrected light from the array into inexpensive, single-mode, polarization maintaining silica fibers, which are then passed via a vacuum feedthrough into a cryogenic dewar operating at 220 K for imaging. MYSTIC utilizes a high frame rate, ultra-low read noise SAPHIRA detector, and implements two beam combiners: a 6-telescope image plane beam combiner, based on the MIRC-X design, for targets as faint as 7.7 Kmag, as well as a 4-telescope integrated optic beam-combiner mode using a spare chip leftover from the GRAVITY instrument. MYSTIC is co-phased with the MIRC-X (J+H band) instrument for simultaneous fringe-tracking and imaging, and shares its software suite with the latter to allow a single observer to operate both instruments. Herein, we present the instrument design, review its operational performance, present early commissioning science observations, and propose upgrades to the instrument that could improve its K-band sensitivity to 10th magnitude in the near future.

Keywords: Optical interferometry, K band, Protoplanetary Disks

1. INTRODUCTION

The Center for High Angular Resolution Astronomy (CHARA) array,[1] located on Mount Wilson, California, provides six 1-meter telescopes in a Y-shaped configuration, spanning baseline separations ranging from 34 m to 331 m. Whereas most instruments at CHARA use a subset of the array telescopes at a time for improved sensitivity, the Michigan InfraRed Combiner (MIRC),[2] commissioned in fall 2005, was designed to collect simultaneous fringes from all 15 baseline pairs across the near-infrared (J, H, and K bands). With new scientific opportunities made available by the expanded uv-plane coverage, MIRC quickly became the most used instrument at CHARA.

In June 2017, the MIRC camera was upgraded to take advantage of the ultra-high speed, sub-electron read noise, HgCdTe avalanche photodiode SAPHIRA[3] detector, implemented in the C-RED One camera by First Light. This upgrade provided improved sensitivity for faint and extended objects.[4] Concurrently, a redesigned image plane beam combiner was implemented, using single-mode, polarization maintaining optical fibers and

---

Further author information: (Send correspondence to B.R.S.)
B.R.S: E-mail: bensett@umich.edu

an 80/20 beam splitter for recording photometric information of each beam. These improvements allowed the photometric signal to be robust to temporal drifts, and reduced some polarization effects. The beam combining optics were installed in the lab at room temperature, and the upgraded instrument was limited to operate at J and H bands only due to high thermal background in the K band. Over the course of the next year, most of the remaining optics in the beam train were updated culminating in the re-branded MIRC-X instrument, fully commissioned in September 2018.[5]

The Michigan Young STar Imager at CHARA (MYSTIC) was designed alongside the MIRC-X upgrade and by the same team. MYSTIC is a cryogenic, K-band (1.95 μm–2.38 μm) instrument utilizing a C-RED One camera like its sister instrument MIRC-X. The instrument provides two beam combiners inside its cryostat: an all-in-one (AIO) six-telescope image plane combiner, based on the MIRC-X instrument design, and a cross-talk resistant, four-telescope pairwise (ABCD) integrated optic chip combiner which was initially created as a spare the GRAVITY instrument.[6] MIRC-X and MYSTIC share an optical bench at CHARA (see Figure 3), and while it is possible to operate the two instruments independently, both instruments use a shared software architecture enabling a single observer to operate both instruments simultaneously. MYSTIC was first commissioned on-sky in July 2021, with the AIO mode made available to all observers with MIRC-X programs. The ABCD mode was later commissioned in May 2022.

This manuscript is organized as follows. In Section 2, we discuss the primary science cases which drove the design of MYSTIC, with the resulting technical requirements presented in Section 3. We then proceed to describe the hardware of the instrument, discussing the warm optic system in Section 4, the cryogenic dewar in Section 5, and the cold optic system in Section 6. Next, we provide an overview of the operational software in Section 7. In Section 8 we discuss the real world performace of the instrument and demonstrate preliminary on-sky observations. We end the paper with concluding remarks in Section 9.

2. SCIENTIFIC DRIVERS

MYSTIC is built to operate in tandem with the J/H-band MIRC-X instrument, enabling robust fringe tracking even if one instrument measures baselines near a visibility null. Leveraging all 15 simultaneous baselines and 20 closure triangles available at CHARA, MIRC-X and MYSTIC together sample a larger portion the uv-plane at higher spatial resolution than any other current long-baseline facility in a single pointing (An example of the uv-coverage available in a single night's observing with MIRC-X and MYSTIC is shown in Fig 1). This opens new avenues for high angular resolution astronomical research not possible with other instrument facilities, particularly in the realm of model independent imaging.

As its name implies, MYSTIC is designed to probe the inner regions of the protoplanetary disks surrounding young stellar objects (YSOs). MIRC-X and MYSTIC together provide sufficient information to conduct rudimentary snapshot image reconstruction of dozens of T-Tauri (young solar analogues, $<2\,M_\odot$) and Herbig Ae/Be (young intermediate-mass stars, $2\,M_\odot$–$10\,M_\odot$) systems at low spectral resolution ($R \sim 50$ to 100). The wide spectral band coverage afforded by these two instruments will allow for the identification and characterization of features within these disks, including inner disk warps and misalignments, orbiting features, localized vorticities, as well as regions of gas or dust dominated emission. These studies will critically inform planet formation models and reveal reveal temporal phenomena responsible for shadowing variability seen in stellar disks on large scales. Our primary goal for MYSTIC is to extend observations of all Herbig Ae/Be targets observable by MIRC-X into the K-band, as well as to study T-Tauri sources, which are too faint for MIRC-X. Previous observations have shown that many nearby YSO disk systems tend to be very resolved for the longer CHARA baselines. While these sources tend to be brighter overall in the K-band compared to H-band, their stellar contribution is significantly lower, with spectra in the Rayleigh-Jeans tail, leading to fringe contrasts often below 10 %. In order to accomplish these goals, particularly probing T-Tauri objects, we require that MYSTIC be capable of observing YSO targets at 7.5 magnitude or fainter in the K-band. Figure 2 illustrates the population of YSO targets in Taurus and the number of targets available to MYSTIC at a given sensitivity.

As a secondary science driver, high precision closure phase measurements at intermediate spectral resolutions ($R \sim 200$ to 1000) allow for the direct detection of Jovian exoplanets. Particularly for MYSTIC, the flux contrast between planet and star is more favorable in the K-band compared to the shorter wavelengths available
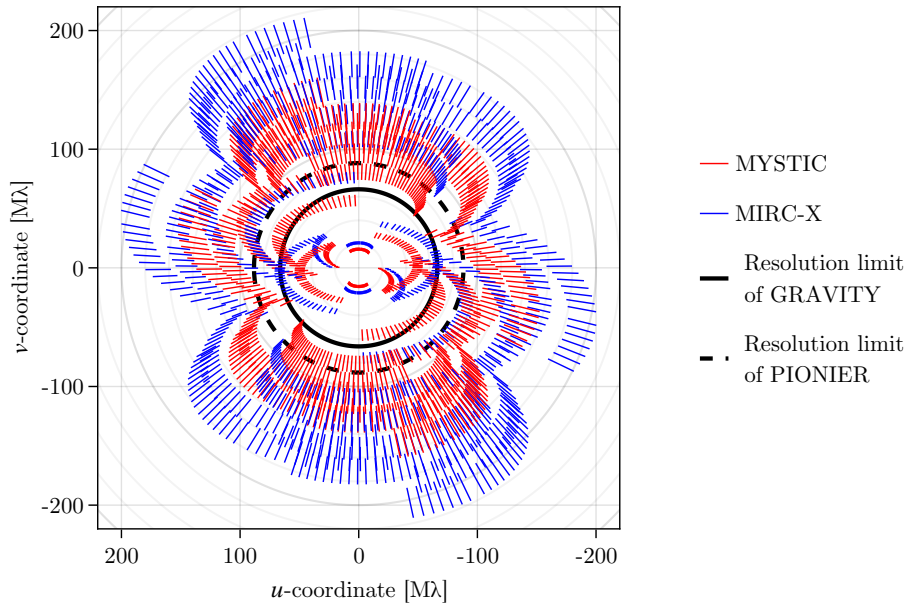
Figure 1. A sample uv-plane track available in a single night for the YSO AB Aurigae. (Note that this figure does not include overheads for collecting calibration data; realistically, this uv-coverage is attainable over the course of two nights.) Utilizing all six CHARA telescopes, MIRC-X and MYSTIC can collect more simultaneous data at higher angular resolutions than any other currently available near-infrared interferometer facility.
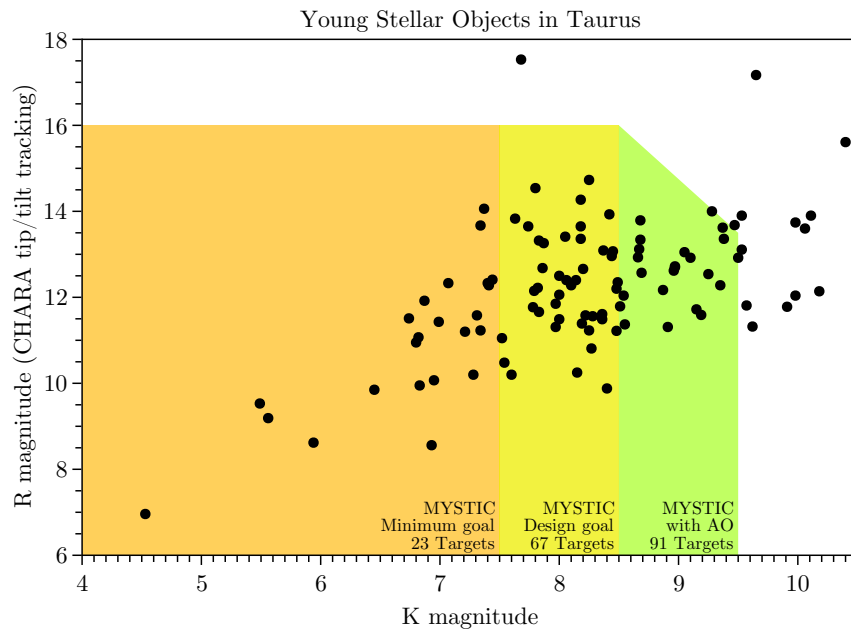

Figure 2. Observable YSO targets in the Taurus-Auriga molecular cloud region[7] for anticipated MYSTIC sensitivity driving instrument design. While MYSTIC currently meets the minimum specification, an increase of 1 magnitude in sensitivity more than doubles the number of available objects for study.

to MIRC-X. For these planetary systems, the spatial resolution afforded by CHARA will make it possible to disentangle the spectral contributions of the star and planet components, allowing for broad characterization of these planet's atmospheres in the near infrared.

Finally, MYSTIC provides a medium spectral resolution ($R \sim 2000$) mode for spectro-interferometry. Within the K-band, spatial resolution of prominent Br-γ ($2.166\,\mu m$) and CO overtone emission ($2.28\,\mu m$ to $2.35\,\mu m$) will enable a direct view of the star-disk connection by probing magnetically driven accretion flows. High precision fringe tracking enabled by MIRC-X will extend available exposure times (on the order of seconds), enabling the study of Herbig Ae/Be emission lines. Complimentarily, high precision fringe tracking with MYSTIC will enable velocity integrated imaging of more prominent spectral lines in the J and H bands accessible by MIRC-X.

3. TECHNICAL REQUIREMENTS

Driven by the science goals mentioned in the previous section, as well as necessary interfacing with MIRC-X and CHARA at large, the following technical requirements constraining the design for the MYSTIC instrument were defined.

1. The detector must deliver a fast readout ($>300\,Hz$) with low noise to allow for coherent integration of fringe visibilities with a high signal-to-noise ratio.

2. The instrument must provide a cryogenic subsystem operating at $220\,K$ for the combiner optics to minimize thermal background in the K-band.

3. The cold and warm optic systems shall be connected by single-mode, polarization maintaining fiber optics to provide spatial filtering. These fibers must provide $>50\,\%$ overall throughput at all wavelengths in the science bandpass.

4. The instrument design must support a six-beam all-in-one combiner as well as a spare four-beam integrated optic combiner chip[8] from the GRAVITY instrument.

5. The entire beam-train and supporting hardware must fit on the shared optical bench with the MIRC-X instrument while minimizing the total number of reflections. Additionally, the layout of MYSTIC should not intersect with CHARA beams headed for the FLUOR instrument, if at all possible.

6. MYSTIC must provide six beam pairwise interference with sensitivity to track fringes with minimal cross-talk at modest spectral resolution ($R \sim 50$) of YSO disks as faint as at least Kmag = 7.5, with a goal of fringe tracking objects as faint as 8.5 mag.

7. The operating software for MYSTIC must integrate tightly with the MIRC-X instrument for coordinated fringe tracking and data collection. A single observer should be able to control both instruments simultaneously with minimal additional burden compared to operating a single instrument alone.

8. To optimize for the image reconstruction of at least 20 T-Tauri objects, and to facilitate the interpretation of temporally varying sources, we require a calibration precision of $<2\,\%$ for square visibility and $<0.1°$ for closure phase measurements at a spectral resolution of at least $R = 20$.

9. At least one strong emission line should be resolvable, ideally probing hot gas near the wind-launching region of YSO sources.

10. MYSTIC must be fully automated system to enable remote operations, including failsafe mechanisms in case of power outages to protect the detector and cryogenic optics. We also require a daily, automatic assessment and report of system health.

4. WARM OPTICS

The warm optics serve to extract the K-band light coming in from the six collimated CHARA infrared beams, to correct for group delay and differential birefringence between the beams, and to inject the light into fiber optics which feed into the cold optic subsystem. This system was designed to use as many off-the-shelf parts as possible, to be as easily accessible for alignment and maintenance, and to share space on an $8' \times 5'$ optical bench with the MIRC-X instrument. Figure 3 shows the layout of the warm optic system on the MIRC-X/MYSTIC optical bench, with all major components labeled. Each component is described in the following subsections.

For reference, we note here that the collimated light beams provided by CHARA are separated $3''$ apart, have a diameter of $19\,\mathrm{mm}$ and include an optical path delay (OPD) of $11.2''$ between successive beams. The common MIRC-X/MYSTIC optical bench is located $6''$ below the center of each of the beams.

Care was taken to design the system with as few reflections as possible, while also fully motorizing all necessary components to enable remote operation by observers. These two goals proved difficult to satisfy simultaneously while also offering two beam combiner modes, so two additional reflections were introduced into the beam path for the ABCD mode; more information is given in Section 4.5.

4.1 Dichroic pickoffs

The first optic on the MIRC-X/MYSTIC table encountered by each of the CHARA infrared beams is a 2-inch dichroic, manufactured by Brinell Vision. The dichroics are placed at a 45° angle of incidence, and reflect K-band light into the MYSTIC optical train, while allowing the H-band light to pass through to MIRC-X at $\geq 90\,\%$
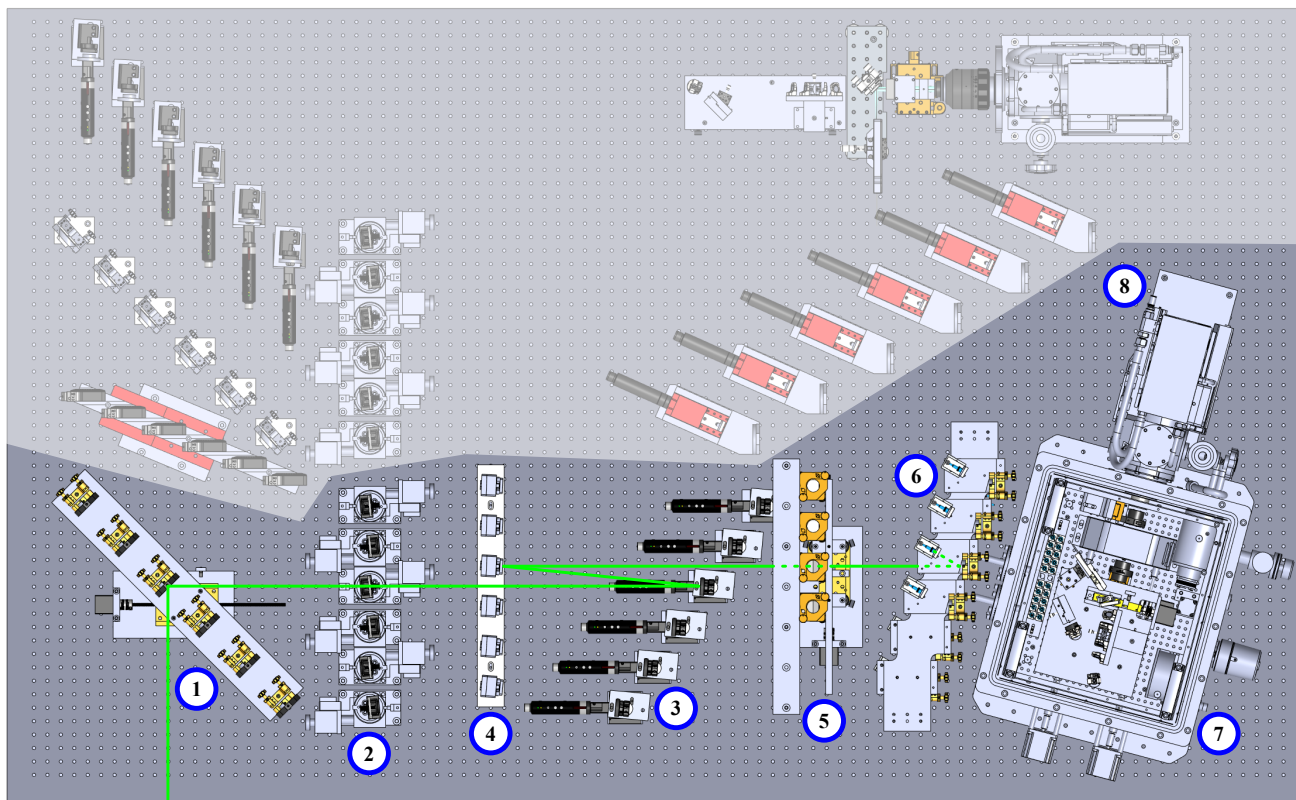

Figure 3. Schematic diagram of the MIRC-X/MYSTIC optical bench. The MIRC-X instrument on the southern side of the table (top in the figure) is faded out to draw attention to MYSTIC. A green line indicates the optical path through the warm optic train along one of the beams. Labeled elements in MYSTIC are as follows: (1) dichroic pickoff assembly, (2) polarization control modules, (3) differential delay lines, (4) tip/tilt control modules, (5) periscope, (6) fiber injection modules, (7) cryostat and cold optic system, (8) C-RED One camera.

efficiency across the bandpass. The incident surface of the 8 mm thick IR-grade infrasil optic has the dichroic coating, and the emergent surface has an anti-reflective coating applied. The optics themselves are mounted in ThorLabs FMP2 optical holders, which are all affixed to a single aluminum plate. Each of these optical mounts has two piezo rotary actuators (Newport Picomotors) for tip/tilt adjustment of the dichroics. These were used for initial alignment of the system, but since the alignment has remained stable, we do not anticipate needing to use them again in the future.

We anticipate that the majority of MIRC-X observers will utilize MYSTIC with their observing programs, even if just to provide additional robustness in fringe tracking. Nevertheless, we envision that there may be situations where K-band observations are unnecessary and the small loss of light in the H-band due to the dichroic is unacceptable. To accommodate this need, we designed a motorized mounting system for the dichroics, allowing them to translate out of the CHARA infrared beams entirely on demand. The common optical mounting plate is attached to a Newport UMR8.51 double ball bearing linear stage which is driven by a Lin Engineering R256-RO stepper motor. A fixed photointerrupter is used as a home switch, which is triggered by a protruding piece of aluminum attached to the linear stage. The assembly is aligned on the optical bench with the home position defined such that the dichroic optics are in the CHARA beams to ensure repeatability of position. With the linear stage moved to its "out" position, a 29.7 mm normal separation between neighboring dichroic mounts is more than sufficient clearance for the 19 mm CHARA infrared beams to pass to MIRC-X unvignetted.

4.2 Polarization control

Differential phase shifts between the horizontal and vertical basis states of light are introduced by mirror reflections in the optical train of CHARA and MYSTIC as well as birefringence in the optical fibers connecting the warm and cold optical subsystems (see Section 4.7). In order to ensure maximum fringe visibility upon beam combination, these differential polarization phase shifts between beams must be corrected. Adopting a similar implementation introduced in the PIONIER instrument,[9] we include a set of 4 mm thick, z-cut lithium niobate plates (LiNbO$_3$), custom fabricated by Crylight Photonics, in the beam path. Birefringence control is then attained by rotating the plates relative to each other, effectively increasing the projected thickness of the material. In the K-band, these provide an adjustable phase shift of up to 5 wavelengths, while providing >99 % transmission across the bandpass for incidence angles up to 30°.

Duplicating the design of the MIRC-X instrument, the lithium-niobate plates are mounted on OES AY110-60 rotary stages, providing a resolution of 0.02°. Each axis is controlled by an R256 by Lin Engineering stepper motor, and is set with a home position oriented normal to the incoming beams.

Figure 4 shows the polarization control modules. For regular operation, the lithium niobate plates are rotated to a nominal position of 20° and then are optimized for optimal fringe contrast using the internal light source. This operation consists of fixing the orientation of a reference beam's plate while slowly rotating the other plates and measuring the visibility of each beam with the reference. The non-reference plates are then moved to the maximum contrast positions. We find that, in general, the plate positions found with the internal light source conform well to the sky. Figure 5 illustrates an example of this operation.

4.3 Differential OPD correction

To maintain mutual optical delay between the MIRC-X and MYSTIC, the next set of 1″ gold fold mirrors are motorized for differential OPD correction. Adopting the differential delay line apparatus of the MIRC-X instrument, the mirrors are translated by Newport 460P-X linear stages and driven by Zaber T-LA28A motors (see Figure 6). This combination enables a total travel range of 1 inch in the east-west direction, with a step size of 1 μm and better than 4 μm repeatability. Unlike their MIRC-X counterparts, the mirrors are mounted in ThorLabs AD1B optical holders which are in turn mounted in kinematic mounts (ThorLabs KS05). The kinematic mounts are themselves not motorized; they were used to fine-tune the alignment during instrument commissioning.
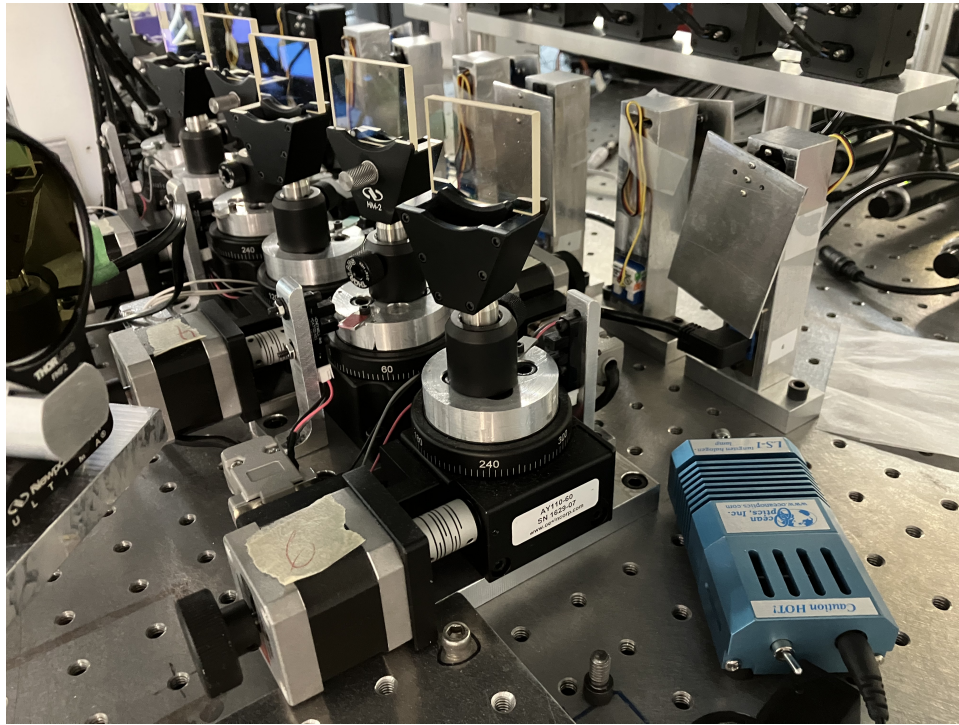
Figure 4. Correction of differential polarization phase shifts between the horizontal and vertical basis states is corrected by a series of rotating lithium niobate plates.
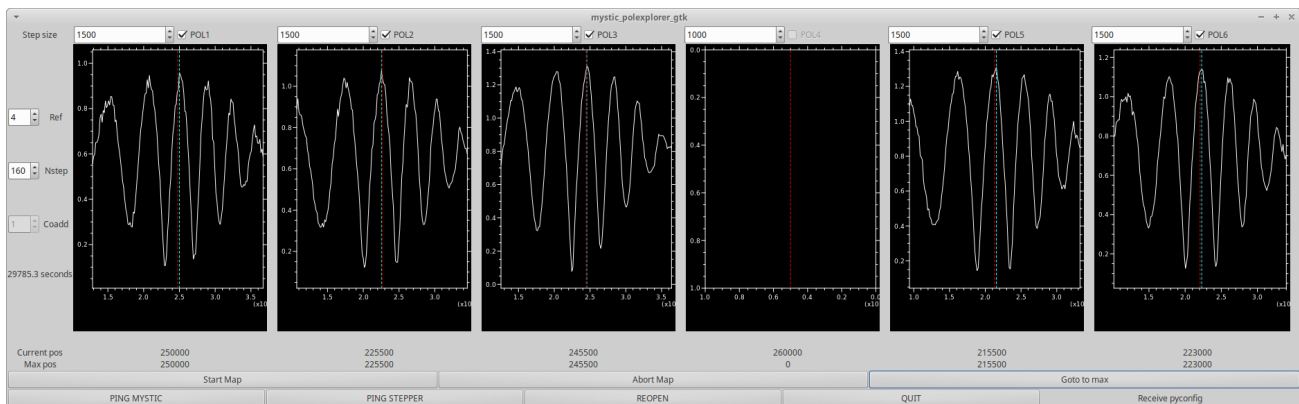

Figure 5. We demonstrate the birefringence correction using the MIRC-X six beam calibration source (STS). In this example, the LiNbO$_3$ plate in beam 4 is fixed as a reference at approximately 20° while we scan the other plates over 160 positions spanning a range of 18.75°, measuring the fringe contrast between beam 4 and each of the other beams at each location. Each plate is then set to the position where visibility is maximized.
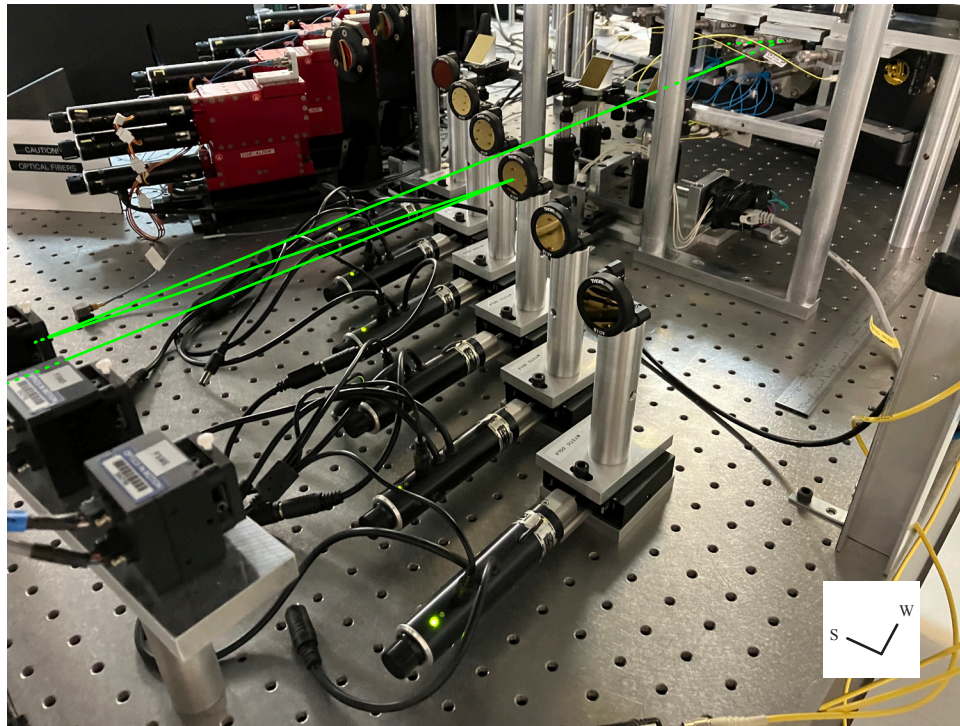
Figure 6.   Optical path delay adjustments necessary for co-phasing MYSTIC with the MIRC-X combiner (and future SPICA instrument) is accomplished via a series of linearly translating fold mirrors.

4.4 Tip/tilt correction

Since the beam guidance for the CHARA array is conducted for visible light and far upstream of the beam combining tables, atmospheric differential refraction causes the beams to drift in the infrared over timescales of several minutes and over angular scales as high as 1 arcsec.[10] Thus, to ensure optimal flux injection into the cold optic system, this tip/tilt error must be corrected for as often as possible while minimizing operational overhead.

To account for these drifts, so that light can be reliably injected into the fiber optics connecting the cold and warm optic systems, we employ a series of magnetic coil-driven OIM5001 Fast Steering Mirrors (FSMs) from Optics in Motion (see Fig. 7) with a $\pm3°$ angular range and 0.25 arcsecond resolution, corresponding to a tip/tilt correction resolution of approximately 10 mas on-sky (which is fine resolution compared to the diffraction limit resolution of a 1-meter telescope: about 0.5 arcsec in K-band). These provide some advantages over the fiber injection strategy employed by the MIRC-X instrument, where each fiber tip is placed on an XYZ motorized translation stage and moved to accommodate a drifting focal point. The FSMs enable better coupling with the fiber tips as they correct the collimated beam shear angle before it is focused onto the fiber, ensuring that the principal ray becomes concentric with the fiber tip core. Since the fibers do not move in the MYSTIC design, there is less opportunity for changing stress birefringence in the fiber, providing stable polarization control. Moreover, since changes in to the FSM angle occur nearly instantaneously (<20 ms including communication overhead), scanning for the incoming flux angle is quicker than in the MIRC-X instrument where the fiber injection motors need time to arrive to position. That said, we do note a few disadvantages using these FSMs to deliver light to the optical fibers compared to the MIRC-X approach. Most notably, the motor controllers produce a non-trivial amount of heat, causing the plastic housing to begin to melt if they are left on for long periods of time. Since space constraints require the controllers for all six FSMs are in very close proximity to each other and other electronics above the MIRC-X/MYSTIC table, they are powered down during daylight hours to prevent damage. The FSMs do not maintain their positions when powered-off, and need to be re-aligned after each power cycle. We have also noticed, on rare occasions, sudden drifts in the mirror positions, but we have not yet isolated whether the mirrors, controllers, or voltage source are the issue.
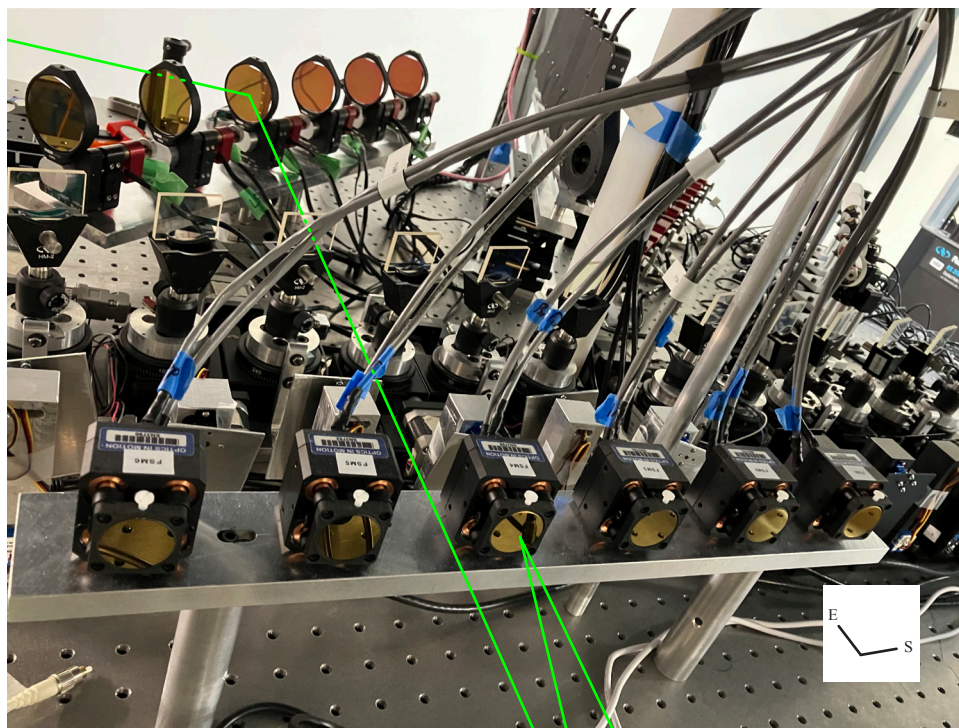
Figure 7. Fast Steering Mirror (FSM) modules, shown near the bottom of the image, are used for tip/tilt correction.

The FSM modules themselves are 1.6 in wide, allowing the light traveling from the polarization control to the OPD correction optics to pass between them unvignetted. The motors contain unprotected gold mirrors and are mounted with a custom 3D-printed mount as the original mirrors, which were glued into the FSM assembly, contained large wavefront errors due to the epoxy stress.

4.5 Periscope

Two additional reflections in a periscope arrangement are introduced into the warm optic beam train for the ABCD combiner mode, allowing each combiner to have dedicated fiber injection hardware. A Lin Engineering R256-RO stepper motor drives the lower half of the periscope assembly, with all of the lower 45° gold-coated wedge mirrors mounted on a common Newport UMR8.51 linear translation stage, moving in the north-south direction (orthogonal to the beam propagation). These mirrors, when inserted into the beam path, redirect the light upward to another stationary set of 45° mirrors, which restores the former (westward) propagation direction, directing the light toward the ABCD fiber injection modules. Alternatively, with the lower 45° mirrors translated out of the beam path, the light travels toward the AIO injection modules. Figure 8 illustrates the periscope assembly.

4.6 Fiber injection

Each collimated light beam is reflected off of an off-axis parabola (OAP) which focuses the light onto the tip of a fiber optic (fibers are described in the Section 4.7). The OAPs were selected to produce a 30° reflection with an effective focal length of 54.45 mm to accommodate the acceptance cone of the fiber optics. We initially tested off-the-shelf gold coated OAPs from Edmund optics (Stock #35-491), but found that they produced significant coma aberration at optimal image quality in our setup. We then ordered a set of custom diamond cut OAPs, delivered by Nu-Tek Precision Optical Corp, with the same dimensions as the aforementioned Edmund mirrors and a surface figure of $< \lambda/20$ RMS at 632.8 nm. These mirrors did not show low order aberrations and concentrated the light into a smaller spot upon focus. Figure 9 illustrates the image of the reflected light for
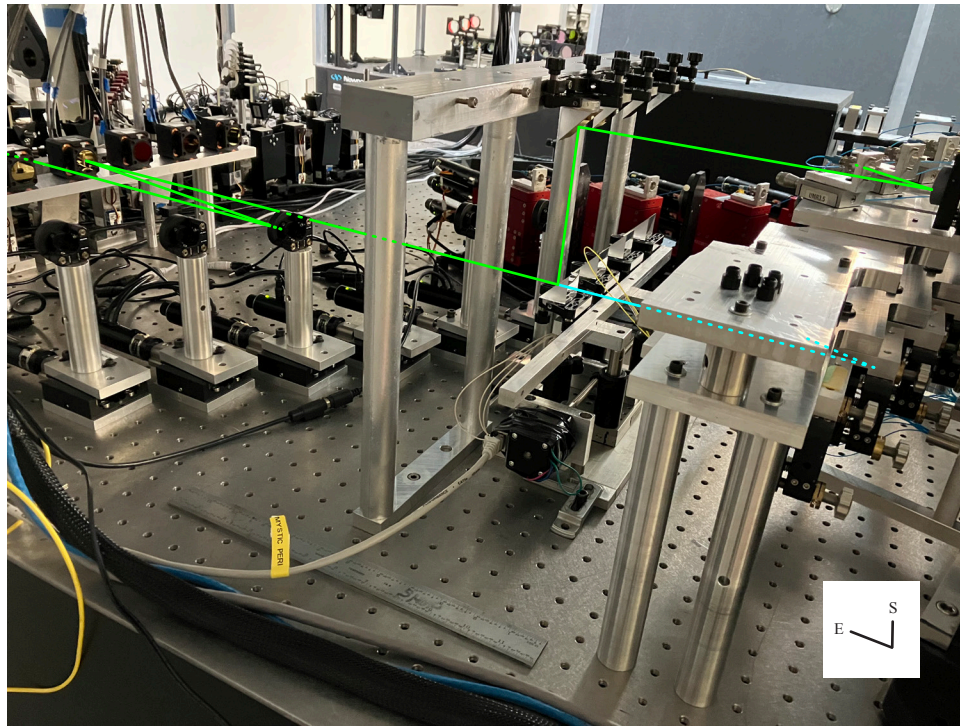
Figure 8. The periscope assembly is shown in the center of the image. The bottom 45° mirrors slide in/out of the infrared beams, allowing light to be directed up to the ABCD fibers (green path) or past the periscope assembly toward the AIO fibers (cyan path).

both mirror stocks. Each of the ten fiber injection modules (six for AIO mode and four for ABCD mode) are equipped with a Nu-Tek OAP.

The fibers themselves are each connected to an L-bracket which is placed on a manually operated translating stage (Newport UMR3.5) to provide focus adjustments during initial alignment of the system. The OAPs were mounted into Newport 1-inch optic holders with two degrees of freedom for tip/tilt adjustment. Each injection module (see top of Figure 10) consisted of a plate hosting the OAP mount and fiber holder, with the latter centered on the primary ray as reflected from the nominal OAP position at a distance of 55 mm from the mirror surface. Image quality optimization of each injection module was then accomplished by back-projecting visible laser light through the fiber optic while adjusting the tip/tilt and rotational orientation of the mirror until the smallest spot size of the re-imaged emergent collimated beam was obtained. Once the OAPs were aligned, the tip/tilt adjustments were locked in place. Individual injection modules for each combiner mode were mounted together on a single plate, with the AIO mode modules hanging on the underside of the plate and the ABCD mode modules on a second plate above. The bottom of Figure 10 shows this common mount for the AIO mode injection modules.

4.7 Fiber optics

Optical fibers are employed in MYSTIC to transport light from the beam combining lab into the cryogenic dewar. In each CHARA beam, light travels through three connected fibers: first via a patch cable linking the injection modules to an external plug-plate, then through a vacuum sealed feedthrough tube traversing the cryogenic dewar wall to an internal plug-plate, and then finally into a set of fibers glued into the all-in-one v-grove module (see Section 6.1) or the ABCD optical chip (see Section 6.2). A three fiber train was chosen instead of a simpler one or two fiber system to facilitate better overall length-matching and to prevent accidental breakage of the feedthrough fibers during testing, despite a greater injection loss due to the additional coupling.
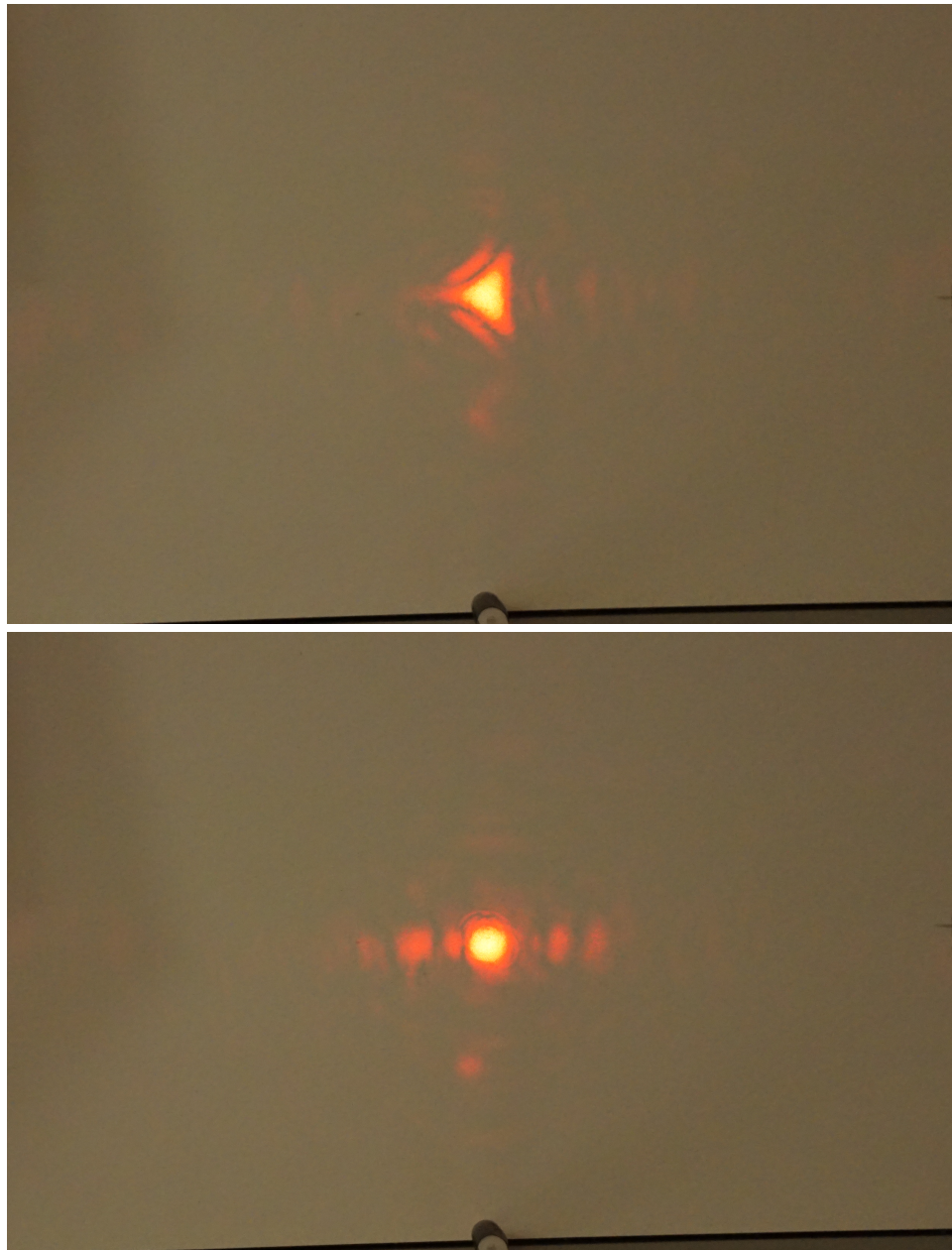
Figure 9. A HeNe laser signal is emitted from a fiber optic at the focal point of each OAP; the images above show the resulting collimated beam refocused of (top) an off-the-shelf OAP mirror produced by Edmund (Stock #35-491) and (bottom) a custom fabricated OAP by Nu-Tek. The former produces a strong coma whereas the latter produces a smaller overall spot and does not display significant low order aberration.
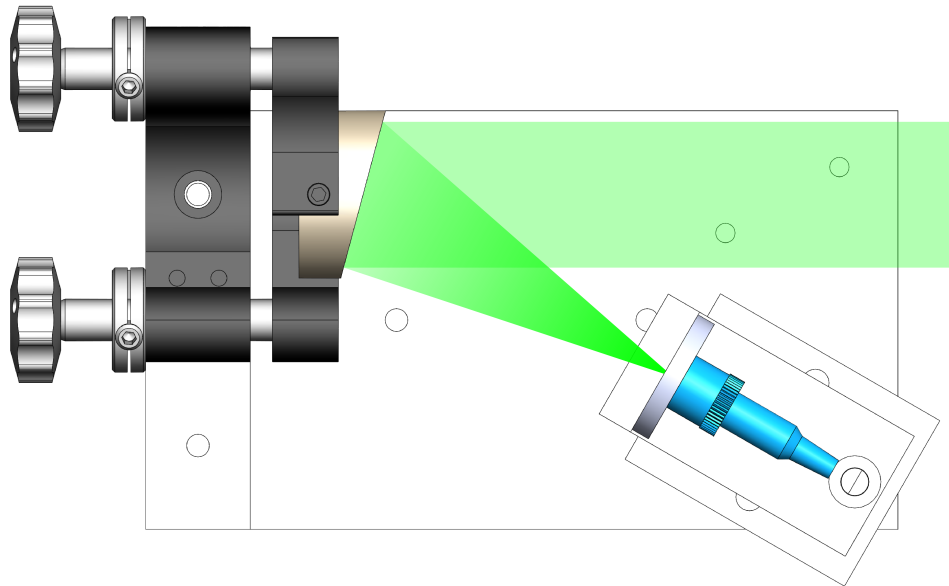
Figure 10. (Top) Schematic view of the fiber injection mount. CHARA beams are reflected by a gold coated off-axis parabola and focused onto a fiber tip. (Bottom) View of the six fiber injection modules for the AIO combiner mode, hanging from mounting plate. Four additional fiber injection modules for the ABCD combiner mode are mounted on a plate above (see far right side of Fig 8).

Table 1. Properties of Nufern PM1950 Silica Fibers

Property	Value
Core NA	0.2
Cutoff wavelength	$1.72\,\mu m$
Mode field diameter at $1.95\,\mu m$	$8.0\,\mu m$
Core diameter	$7\,\mu m$
Beat length at $1.95\,\mu m$	$5.2\,mm$
Throughput/meter at $2.2\,\mu m$	$94\,\%$
Throughput/meter at $2.37\,\mu m$	$85\,\%$

The fibers were selected to be single-mode,[11] acting as a spatially filter removing non-zero photon orbital angular momentum (POAM) modes introduced into the wavefront signal by atmospheric turbulence, and polarization maintaining, to ensure temporally stable fringe contrast between the horizontal and vertical polarization modes as measured by the detector. Furthermore, the chosen fiber was required to accommodate the ABCD combiner chip with a numerical aperture of 0.19. After internally testing several off-the-shelf optical fibers, Nufern PM1950 silica-based fibers were selected for use in MYSTIC as they provide a high throughput throughout K-band, suffering low OH absorption at longer wavelengths. Table 1 summarizes measured properties of these fibers. Compared to the flouride-glass fibers used in the GRAVITY instrument, PM1950 fibers exhibit minimal bending losses, exhibited overall higher throughput, and were more cost effective and less delicate than their counterparts.

To mitigate visibility loss due to differential dispersion between fiber trains, each fiber set was cut and connectorised to a consistent length by Costal Connections. The lengths of all available fibers were measured using a Luna optical backscatter reflectometer, with typical fibers in each set matched within 0.5 mm. We then determined the optimal combinations of fibers for each train to minimize the total length difference and thus minimizing chromatic dispersion. For the all-in-one combiner, the longest train exceeds the shortest by a length of 73 µm, with a typical difference between trains of 23 µm. For the ABCD combiner, the greatest difference is 2.15 mm with a typical difference of 0.88 mm.

The vacuum feedthroughs for both combiners were also produced by Costal Connections. Each feedthrough was created with a total of 9 length matched, connectorised fibers vacuum sealed with an epoxy. The extra cables allowed us more flexibility in choosing optimal fiber combinations for each beam. That said, we were remarkably impressed by the consistency of the final lengths Costal Connections were able to achieve in all of these fibers.

Except for the final glued connection, each fiber end is terminated by an FC/PC connector. After cleaning the fiber tips, a typical 5 % to 10 % throughput loss at each connection could be achieved, with the net throughput varying within this range each time cables were unconnected and reconnected together. Overall, a total throughput of 60 % to 80 % was measured for each fiber train across the K-band, with each train including two intermediate fiber connections, and a total fiber length of 101.0 cm for the AIO mode fibers and 98.5 cm for the ABCD mode fibers. We found that the FC/PC connectors designed for vacuum applications, with a hexagonal shaped thumb screw, could be connected and disconnected with ease in tight spaces, while mitigating risk of damaging the fibers, with the aid of a flare nut socket.

5. CRYOGENIC DEWAR

The interferometric beam combination of MYSTIC occurs within a custom designed rectangular cryogonic vacuum dewar, built by Universal Cryogenics, to mitigate thermal background from the lab in the K-band. The cold optic system, described in Section 6, is placed within the cryostat, built on top of a $15'' \times 13''$ cold plate. The space between the outer and inner wall of the dewar is filled with several layers of superinsulation (MLI) to reduce the thermal load on the cooling system. The dewar includes the following interfaces: two 2.75'' ports for the fiber optic feedthroughs, a DN100 port for the externally mounted C-RED One camera, two external stepper motors driving the internal filter wheel (see Section 6.3) via a ferrofluid interface, an electronic feedthrough, a vacuum feedthrough, and hose connections for the cooling system. Access to the inside of the dewar is facilitated by a removable lid. Figure 11 shows an inside view of the cryostat.

While in operation, the dewar is maintained at a pressure of roughly 6×10^{-6} mbar. The vacuum is provided by a turbo pump. The initial pump down from atmospheric pressure is usually completed over the course of several hours, but may take up to a few days if the dewar has been at atmosphere for an extended period of time. We believe this is predominantly due to air trapped within the superinsulation layer, which subsequently takes a long amount of time to finish out-gassing. If we were to design the instrument again, we would opt for several layers of aluminum plate between the inner and outer walls of the cryostat instead. Like MIRC-X, MYSTIC's vacuum systems are equipped with electromagnetic valves which close during a power outage (and must be manually reopened).

Once the internal pressure of the dewar reaches 10^{-3} mbar, the cryostat is cooled by a Polycold Compact Cooler from Brooks Automation with Standard grade NF-55 refrigerant. Since this fluid would continue to cool the system to 183 K, far lower than our specifications demand, a small heater is placed inside the dewar to actively maintain an operating temperature of 220 K. An aluminum shield is placed between the the optical elements and the cooling coils and heater in order to prevent stray reflections of the K band light emanating from the thermal head from coupling into the beam path. Two thermometers are placed on the optic side of the aluminum shield, which inform a PID loop controlling the thermal head via a LakeShore Model 336 Temperature Controller. In case of a thermal head failure, the temperature controller sends a signal to turn off the cooling compressor if the temperature drops below 219 K. The thermal head is also used for cooling the system from room temperature; to prevent thermal shock of the internal components, the dewar is cooled at a rate of $0.034 \, \text{K} \, \text{min}^{-1}$, which brings the cryostat to temperature over the course of 48 hours.

Between the inner dewar wall and the C-RED One camera window, we inserted a baffle tube comprised of a series of traps (flat rings) of varying inner diameters in an attempt to minimize stray thermal background light from coupling into the beam path (see Fig. 12). Each of these disks were coated with an application of Singularity Black paint (NanoLab) to maximize light absorption. While this did help in significantly reducing the total thermal background measured by the detector, we still report a 3.6 higher median flux per pixel than anticipated (typical 360 ADU/s, compared to MIRC-X's 100 ADU/s at an operating camera gain of 40). We have concluded that the dominant source of background flux is not coming from within the MYSTIC cryostat, but instead is leaking in from another source into the C-RED dewar. Most likely, this excess light is emission from the sapphire window separating the the camera and MYSTIC dewars, which is not entirely thermally isolated from the lab (see Fig. 13). We will explore avenues to reduce this flux in the future.

6. COLD OPTICS

The cold optics system consists of the beam combiners and spectral dispersing elements, together with a couple motorized optics necessary for aligning the dispersed light onto the detector. Each of these elements, together with the C-RED One camera, are described in the following subsections. A schematic drawing of the optical elements in the cold optics system is presented in Fig. 14.

The cold optic system includes four stepper motors and translation stages inside the cryostat. We found that, after removing grease from the internal bearings of these elements, they work just fine at cryogenic temperatures, bypassing the need to purchase components specifically advertised and priced for cryogenic applications. In lieu of grease lubricating our linear translation stage bearings, we applied a layer of MoS_2 powder to facilitate smooth motion. Operation of these elements was successfully tested inside a cooler filled with dry ice (198 K) before being added to the dewar.

6.1 All-in-One beam combiner

The all-in-one (AIO) beam combiner borrows heavily from the design of the MIRC-X combiner. Herein, we provide a brief description of the combiner, particularly highlighting differences between the MYSTIC version to that of MIRC-X. We note that this design is cross-talk resistant if observing with 5 or fewer telescopes. For a more in-depth discussion on the design of the AIO combiner, we refer the reader to Ref. 5.

Fiber optics carrying light from each of the six CHARA beams are arranged vertically in a non-redundant spacing on a silicon V-groove by OZ Optics, in slots 4, 6, 13, 18, 24, and 28 with a 250 µm pitch, providing a unique spatial frequency in the subsequently interfered light for each pair of beams. The fiber ends are glued
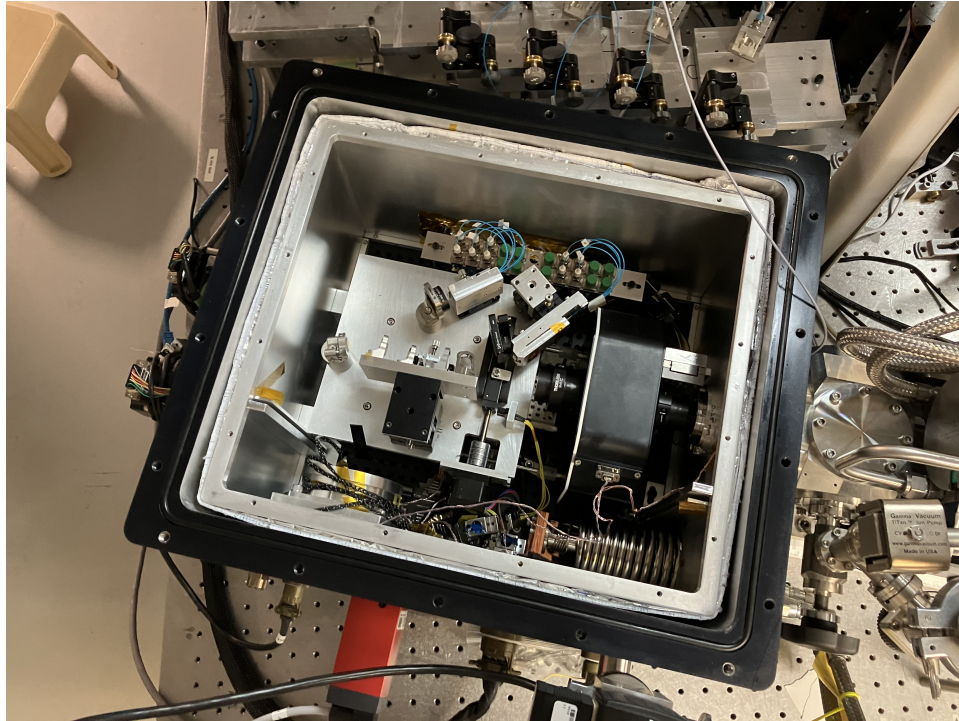
Figure 11. An inside view of the MYSTIC dewar (note that the aluminum sheet which blocks thermal photons emitted directly from the heater is removed). At the top of the image, inside the dewar, is a fiber plug plate, with the vacuum feedthrough fibers connected on the underside. The group of fibers to the left connect to the AIO V-groove where the light is then reflected into the AIO combiner immediately below. The group of fibers on the right connect directly to the ABCD combiner.
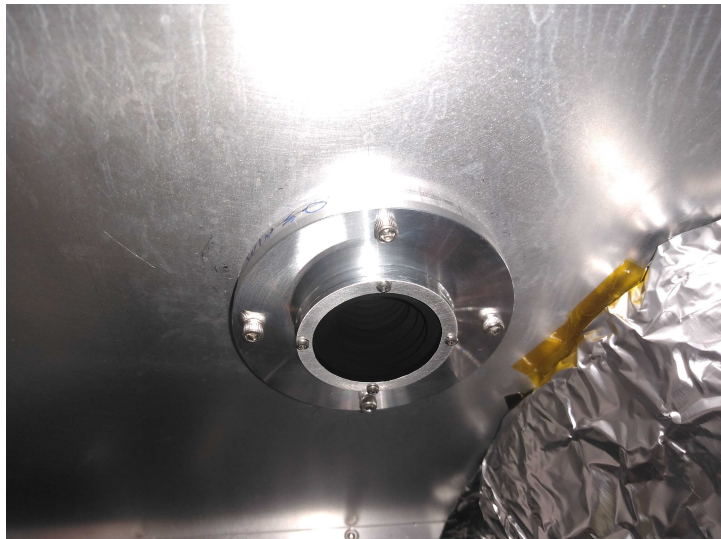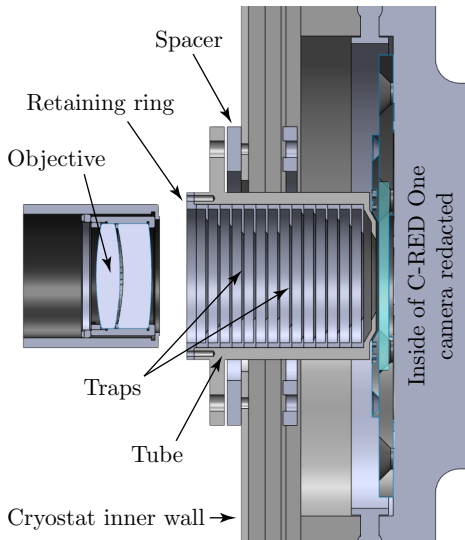

Figure 12. Position and schematic cut view of the baffle tube assembly (left) and an image of the baffle tube mounted on the inner wall of the MYSTIC cryostat (right). The baffle tube consists of a series of varying inner-diameter traps coated in Singularity Black paint, which absorb stray thermal background light.
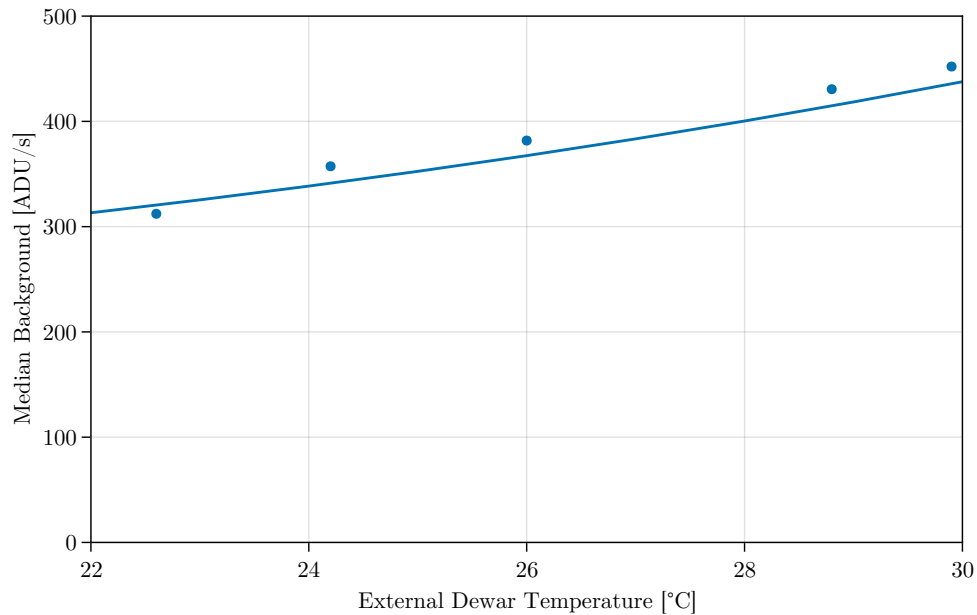
Figure 13. Median pixel count of the background with the detector set to a Gain of 40. By heating the external case of the dewar, we see additional thermal light coupling into the detector. The roughly fit line illustrates blackbody thermal light coupling into the camera chamber in excess of a nominal 150 ADU/s background.
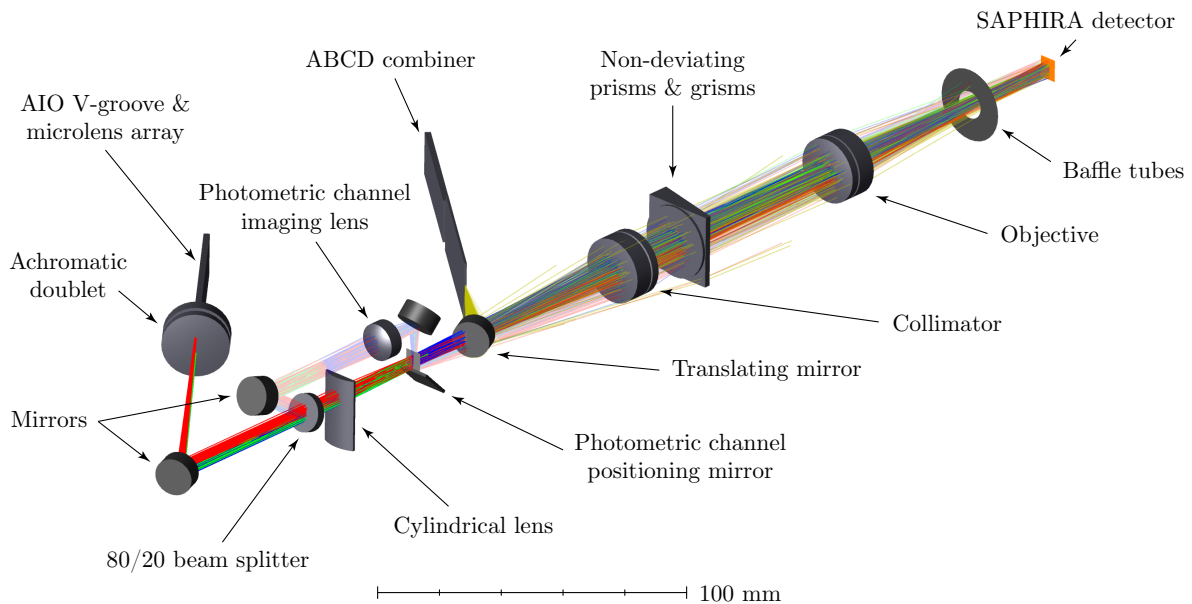

Figure 14. Annotated layout of the cold optic system, with beam trains for both combiners overlaid. To the left of the translating mirror are the AIO mode optics. This mirror slides out of the beam train for AIO mode observations, or into the beam train for ABCD mode observations.
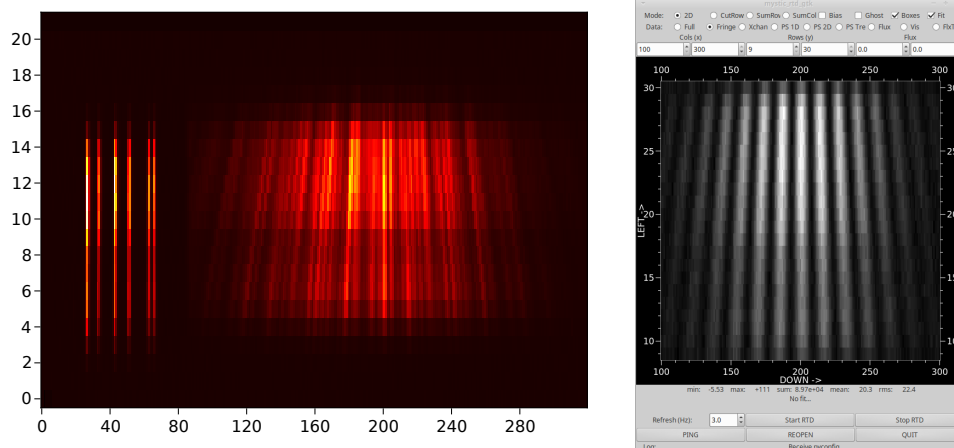
Figure 15. A typical detector readout with six telescope delay in AIO mode is shown in the left image. Photometry is measured at each wavelength channel on the left of the detector readout and interferometric fringes are formed on the right, with the fringes of all 15 baselines superimposed at non-redundant spacial frequencies. The screenshot on the right shows an example of a fringe pattern with two beams only.

to a microlens array which collimates the fiber outputs. The micro-lens array was custom made by Mackinac MicroOptics to accommodate the higher numerical aperture of the MYSTIC fibers. The array consists of 48 fused silica spherical lenses spaced in a single line 250 μm apart, with the diameter and radius of curvature of each lens also 250 μm, all on a 0.729 mm thick IR-grade fused silica substrate. These micro-lenses were then carefully aligned with a Fabry-Perro interferogram and glued in place.

The collimated beams are then focused by a 200 mm achromatic doublet (Thorlabs ACA254-200-D) which yields a highest frequency sampled at the detector of 2.64 pixel/fringe at 1.9 μm. As the beams converge a reflection redirecting the path is introduced to keep the system within the constraint of the dewar followed by a beamsplitter which extracts 20 % of the light from each beam for subsequent photometric measurement. The remainder of the light continues through a cylindrical lens near the focal point, emulating a slit where the interference pattern is generated. The CaF_2 cylindrical lens used here is leftover from the original MIRC instrument, with a 30 mm focal length. Following the cylindrical lens, the previously extracted photometric light is re-imaged and then directed via mirrors below and parallel to the primary ray of the interfered light where both pass on to the spectrograph collimator (Section 6.3). A typical detector image with the AIO mode in optical delay is shown in Fig. 15 with fringes from all 15 baselines overlayed on top of eachother and with the photometry measurements beside. We note that there is an approximate 1 pixel shift in the spectral direction between the fringes and the photometric channels.

6.2 ABCD beam combiner

The ABCD combiner is a spare integrated optics chip produced for the GRAVITY instrument.[6] It conducts a 4 beam pairwise (6 baseline pair) ABCD combination whereby the fringe contrast for each baseline pair is sampled at four phases in quadrature, allowing the instantaneous complex visibility to be measured. We refer the reader to Ref. 8 for a more in-depth discussion of the chip itself.

The chip's 24 outputs are separated by 7.5 pixels on the detector (see Fig 16). A custom microlens array, consisting of 72 lenses, each with a diameter and spacing of 180 μm, a radius of curvature of 200 μm, and a thickness of 0.450 mm, was manufactured on a IR-grade fused silica substrate by Mackinac MicroOptics to adapt the chip's output f-numbers from $f/2$ to $f/12$. The microlens array and a set of PM1950 fibers arranged in a V-groove were assembled with a UV polymerized glue (Epo-Tek OG142-87) onto a common mechanical support (see Fig. 17).

The final assembled beam combiner was mounted just behind the AIO combiner assembly. A 1″ gold mirror, placed on a Newport 422-1S linear translation stage and actuated by a Nema 14 stepper motor (JK 35HY26-0284),
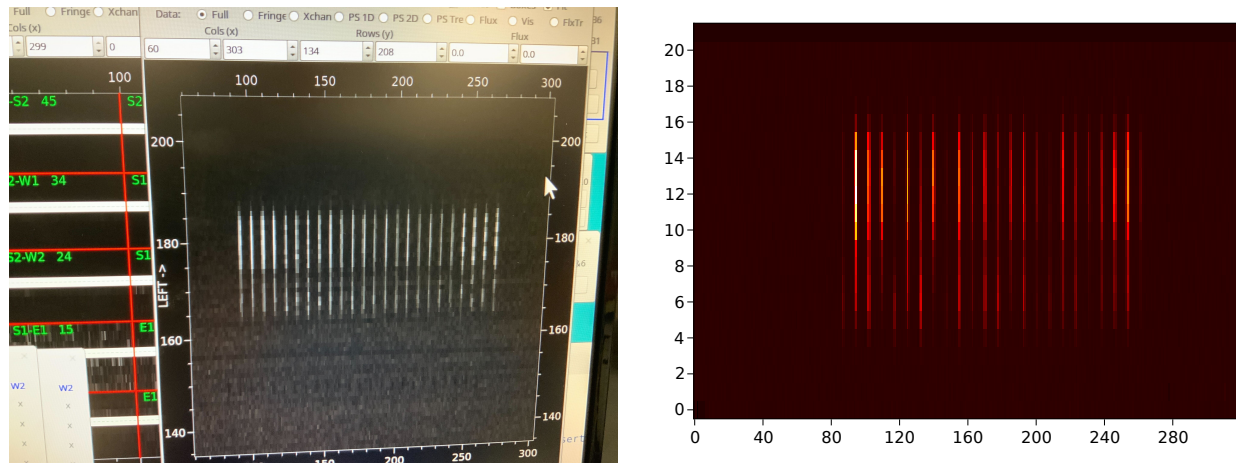
Figure 16. ABCD chip observations appear on the detector as a series of 24 parallel lines, measuring four phases of the visibility contrast at each wavelength channel. In the example shown on the left, several outputs show regular light and dark bands along the spectral direction, indicating unoptimized optical path delay at the time this photo was taken. In the snapshot shown on the right, the optical path delay is corrected and for each baseline, the ABCD outputs show varying flux intensity indicitive of measured fringe contrast.
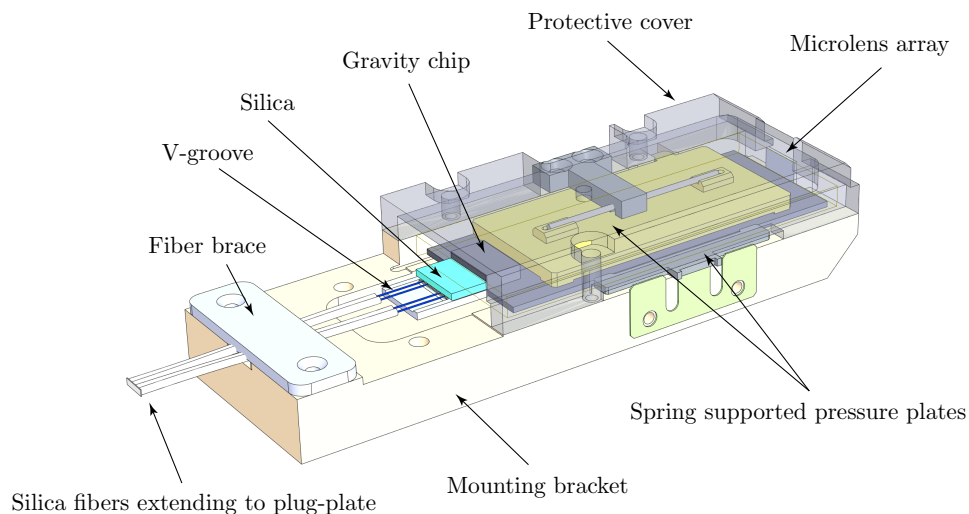

Figure 17. Schematic of the ABCD combiner assembly. Note that the cover protecting the GRAVITY chip from incidental damage is made transparent in the diagram for illustrative purposes only.

is used to either reflect light from the ABCD chip into the optical path immediately before the spectrograph collimator, or allow light from the AIO combiner to pass through instead.

6.3 Spectrograph

Following the beam combiners, MYSTIC includes a spectrograph consisting of a collimating optic on an XZ linear stage (spectral and focal direction), two filter wheels – each with six slots – containing an assortment of dispersive optics, and an objective on a Y linear stage (spatial direction) which focuses the light onto the detector. We note that while having the focus adjustment on the collimator optic is not ideal, the Z location of the objective was carefully positioned for optimal focus at 220 K (determined via Zemax modeling of the system). Moving the collimator in the Z direction is necessary only during engineering tests when the inside of dewar is at lab temperature.

The collimator and objective are both off-the-shelf achromatic doublets (Thorlabs ACA254-100-D) mounted inside Thorlabs SM1 tubes and affixed to motorized Newport 9066-COM linear stages. Motorization is provided by a Nema 14 stepper motor, connected to the stage via a Ruland aluminum beam coupling. Under cryogenic conditions, we notice significant hysteresis in our modified stages, whereby the light positions in the detector typically drift by a pixel after moving the stages a millimeter and then back. Moreover, since the X stage sits atop the Z stage, motions in the latter affect the position of the former on about a 1 pixel level.

The filter wheels are mounted together as a single assembly. Rotation of the wheels is facilitated by external DC stepper motors connected to the wheels via shafts along the base cold-plate of the dewar. The wheels are configured in a 6:1 gear ratio, so a single revolution of the connecting shaft advances a filter wheel by one position. A notch with a spring loaded homing switch marks the position of one of the slots in each wheel. The first wheel has a depth of 15 mm and the second has a depth of 29 mm. Each slot is designed to accommodate a 1″ square optic or a 1″ circular optic mounted inside an SM1 tube (which were cut to length on a lathe). Square optics are held in place by small, thin beryllium copper tabs.

The optical elements filling the wheel slots are enumerated in Table 2. The cold plug consists of Singular Velvet Appliqué (NanoLab) affixed to an aluminum puck, and was used as a thermal background reference. The grisms are all 1″ diameter Schott IRG7 wedges produced by United Crystals Inc., with plane ruled transmission gratings affixed to the wedge surface by Richardson Gratings. The gratings were selected from Richardson's standard catalog. The grisms were mounted inside of Thorlabs SM1 tubes with a cylindrical aluminum shell cut to a matching wedge angle, painted with Singularity Black, and placed inside the SM1 tubes to prevent the grisms from toppling over as the wheel rotates. The grisms are held in place by a silicone o-ring spacer (Marco Rubber T1003-020) and an SM1 retaining ring. The Wollaston prism, produced by United Crystals, is a square optic made of two perpendicularly oriented quartz wedges optically cemented together, producing a ∼1° splitting angle. Since the delivered Wollaston prism was marginally thicker than the depth of the first filter wheel, we 3D printed an 2 mm spacer for the wheel backplate to accommodate the optic.

The non-deviating prism pairs were also produced by United Crystals, with spectral resolutions R of 20, 49, and 100. Each prism was made with in infrasil glass wedge followed by a CaF_2 wedge. In the first iteration of prisms, the optics were square with optical cement holding the wedges together. Upon testing these optics under cryogenic conditions, the CaF_2 halves shattered. Believing that this was due to tight mounting inside the filter wheel which imposed stresses in the optic during thermal contraction, we ordered a second set of prisms, this time circular so that they could be mounted inside SM1 tubes. Again, upon cooling, the CaF_2 halves shattered. We found in the end that the differential thermal contraction between the Infrasil and CaF_2 halves at 220 K produced shear stress on the Calcium Flouride crystal beyond its fracture limit. Thus, in the third iteration, we had the prisms halves made separately without optically cementing them together and 3D printed a thin spacer between the wedge halves before mounting into the filter wheel slots. Unfortunately, with an air gap between the strong wedge angles in the $R = 100$ prism, the Infrasil optic exhibited total internal reflection. To recover this spectral mode, we used a second $R = 49$ prism, so that each filter wheel has one. Modeling the light passing through both prisms in Zemax, we expect a final spectral resolution of $R = 99.5$.

6.4 Detector

At the end of the optical train, a First Light C-RED One camera[12] is affixed to the dewar wall, featuring a 320 pixel × 256 pixel Lenardo SAPHIRA detector[3] with a 24 μm pixel width. The detector operates at a high

Table 2. Filter Wheel Elements

Slot	Wheel 1	Wheel 2
1	Empty	Empty
2	Cold plug	$R = 20$ Prism
3	$R = 278$ Grism	$R = 49$ Prism
4	$R = 49$ Prism	Empty
5	Narrow band filter (1.930 μm)	$R = 981$ Grism
6	Wollaston Prism	$R = 1724$ Grism

vacuum of 10^{-7} mbar and at 80 K, and delivers full-frame readout rates of 3.5 kHz with sub-electron read noise per pixel. Often, only a subset of the full frame is read for typical science configurations, further increasing the raw frame-rate. Several readouts are then averaged per frame,[5] reducing the noise further (and setting an operational frame-rate typically closer to 400 Hz). During an observation, many frames are then readout non-destructively before the pixels are reset.

The vacuum pressure is started by a turbo-pump shared by MIRC-X and MYSTIC cameras, and then maintained by a dedicated ion pump produced by Gamma Vacuum. The camera is cooled down using an internal pulse-tube cryocooler operating at 47 Hz with two coolant hoses connected to an external water chiller maintained at 10 °C. We do see a low-amplitude ($\sim$20 ADU/s RMS) 94 Hz nuisance oscillation in the detector readout related to the pulse-tube operation; this C-RED One was one of the earliest units produced by First Light and newer units have this issue fixed.

Immediately behind a sapphire window isolating the MYSTIC cryostat from the camera's internal vacuum system are three K-band filters which prevent thermal background photons outside of the science bandpass from entering the detector chamber. The first of these filters is custom produced by Brinell Vision, and sets the overall bandpass for MYSTIC, yielding >90 % transmission for 1.98 μm–2.36 μm and <1 % transmission in outside the range 1.81 μm–2.51 μm. Fig. 18 reports the measured throughput of this filter. The remaining two filters were provided by First Light, and prevent photons with wavelengths exceeding 2.45 μm from reaching the detector.

7. SOFTWARE ARCHITECTURE

The instrument operational software was designed from its conception to provide the same interface for operating both the MIRC-X and MYSTIC. Both instruments on a client/server model, allowing any number of GUIs either on-site or remotely to connect to servers running at CHARA. While the MYSTIC camera and data acquisition is conducted on a separate computer to that of MIRC-X, many other servers of the MIRC-X instrument are extended to now include MYSTIC subsystems in a single GUI. For example, the stepper motor server communicates with all DC stepper motors on the entire MIRC-X/mystic table and the vacuum server now monitors the internal temperatures and pressures for both C-RED One cameras and the MYSTIC dewar. We direct the reader to Ref. 5 for a thorough overview of the software implementation.
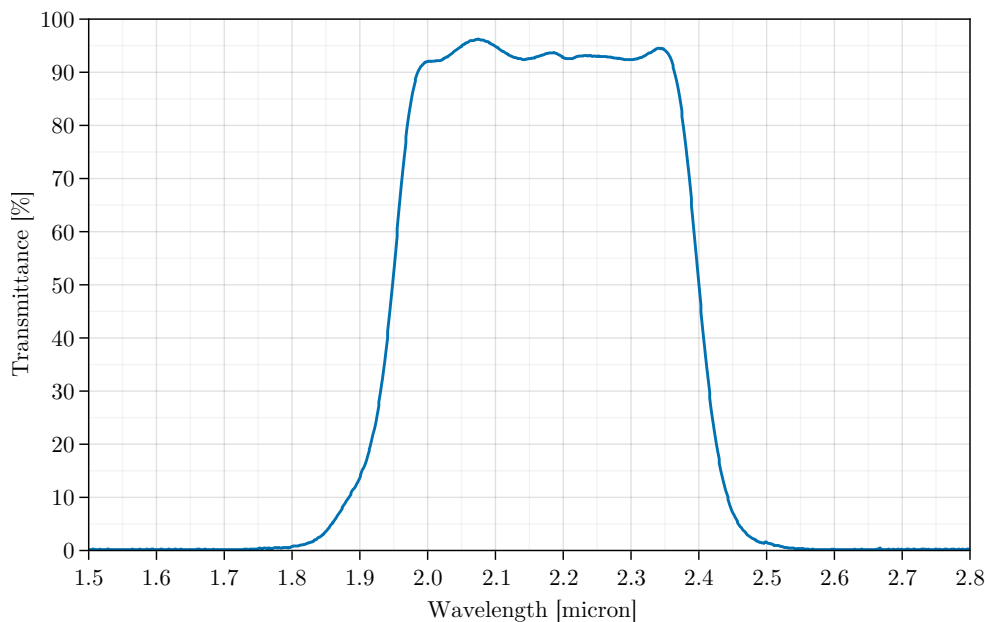

Figure 18.   Measured throughput of the custom K bandpass filter inside the CRED-One camera, produced by Brinell Vision.

A new hardware server was written to control the FSM hardware, which are steered by applying a voltage in the $\pm 10\,\text{V}$ range along each of their axes. The new server communicates with a T7 series LabJack to communicate and log the required voltages.

With the installation of MYSTIC, we have placed four, single axis piezoelectric accelerometers (Brüel & Kjær Type 4507-B-004) on the combined MIRC-X/MYSTIC optical bench to measure vibrations in the system, which are a potential cause for fringe contrast drops. These accelerometers are monitored (Brüel & Kjær Type 3676) and logged by the shared vacuum server, with RMS vibration measurements included in data file headers over the course of a file integration.

The super server, which manages data sequencing and provides a high level interface to other hardware servers to configure instruments for observing and communicating with CHARA servers, has been updated to allow for simultaneous data collection in both instruments. In addition to data, background, foreground, and shutters frames, the super server additionally implements a new sky frame mode. For MIRC-X, it is sufficient to close internal shutters, blocking the CHARA beams from reaching the detector, to estimate the background contribution. However, for MYSTIC, the shutters themselves contribute to the thermal background and are thus unsuitable for data calibration. In this mode, the server requests an offset off of the target to the telescope control loops, to prevent a bias in the background measurement.

The most significant new feature involves simultaneous active fringe tracking of the MIRC-X and MYSTIC instruments together. Delay line control is implemented in two modes. In the first mode, the observer sets one instrument as the primary fringe tracker controlling the CHARA delay lines, with the second instrument adjusting its own independent differential delay lines. In the second mode, flux and contrast information from both instruments are used together to control the CHARA delay lines and internal corrections. We refer the reader to Ref. 13 in these proceedings, which discusses the fringe tracking and subsequent post-processing co-phasing in detail.

Since the AIO combiner mimics the MIRC-X design, and both MIRC-X and MYSTIC employ a C-RED One camera for data collection, minimal changes to the MIRC-X data reduction pipeline* were necessary to accommodate MYSTIC data in this mode. Most notable is the inclusion of sky frames used for background subtraction of the data. The ABCD mode observations are not yet supported by the pipeline. A substantial overhaul of the data reduction library is in progress to both to support reduction these data, as well as to provide more manual control for bad header information correction and bad data rejection.

8. INSTRUMENT PERFORMANCE

MYSTIC has repeatedly demonstrated a fringe tracking limiting magnitude on-sky of 7.5 with the $R = 50$ prism under good seeing conditions (with a record of 7.7 during a night with especially excellent atmospheric seeing). We note that visibility measurements of objects fainter than this magnitude are still feasible, provided that the target is bright enough in the H band for fringe tracking with MIRC-X. Table 3 enumerates the expected limiting AIO mode K-band correlated magnitudes for MYSTIC fringe tracking at all supported spectral modes. At the time of writing, detailed estimates of the ABCD mode limiting magnitudes have not yet been collected.

8.1 Observations of Iota Pegasi

In this section, we examine early on-sky data of the well-known, 10.2 day period binary star system ι Peg with MIRC-X and MYSTIC on 15 September, 2021. These data were collected using all six CHARA telescopes, with the AIO combiner and an $R = 50$ spectral resolution prism. These observations consisted of repeated pointings to the science target, interspersed with observations of several nearby calibrator objects (HD 207978, HD 214458, HD 213178, and HD 213026) to estimate the transfer function.

The data were reduced and calibrated with the MIRC-X pipeline, version v1.3.5-52†. The data were separated into 5 minute epochs and fit to a geometric model composed of two uniform disks with variable diameters, fluxes, and separation. Figure 20 shows a sample of these data points and the subsequent model fits. We find excellent

---

*The MIRC-X data reduction pipeline is available at https://gitlab.chara.gsu.edu/lebouquj/mircx_pipeline.

†At the time of writing, this version is only available on the develop branch of the MIRC-X pipeline repository.
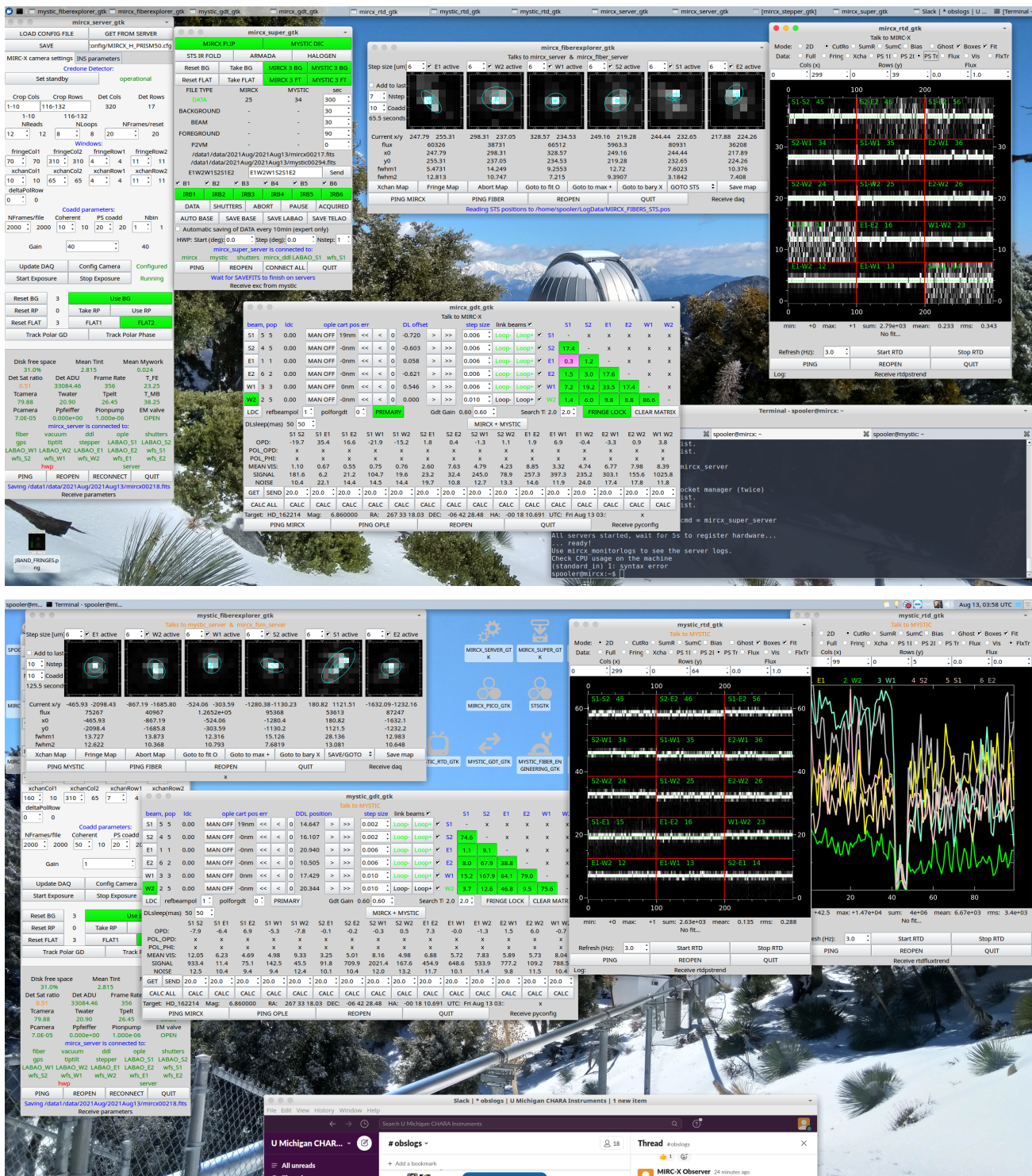
Figure 19. Screenshot of typical six-telescope simultaneous observing with MIRC-X (top) and MYSTIC (bottom). The graphical user interfaces for both instruments function in the same way. MYSTIC windows are distinguished by an orange label at the header.

Table 3. Estimated AIO mode limiting magnitudes without MIRC-X fringe tracking

Optic(s)	R	Kmag
Prism	20	7.9
Prism	49	7.5
2 × Prism 49	100	7.1
Grism	278	5.8
Grism	981	5.1
Grism	1724	4.8

NOTE—Reported magnitudes describe the estimated fringe tracking limit of MYSTIC under excellent atmospheric seeing conditions. If fringe tracking can be accomplished exclusively with MIRC-X, it is possible to integrate fainter targets with MYSTIC. ABCD mode limiting magnitudes have not yet been determined at the time of writing. Using the $R = 20$ prism is only supported for $\leq$ 5-telescope observations in AIO mode due to cross-talk.

agreement between the model and data closure phases. We find that the data reduction pipeline does not well calibrate the square visibility data at the shortest baseline, which is set to the lowest spatial frequency in the MYSTIC AIO combiner and includes crosstalk from the DC spike. Additionally, calibrated square visibilities diverge from model estimates with increasing wavelength. These discrepancies will likely disappear as the data pipeline progresses in development.

Our models of the data find a best fit diameter for the primary star of 1.06 mas and 0.53 mas for the secondary with a K-band flux ratio of 4.43. Overall, these are in reasonable agreement with the canonical parameters of this system (for example, Ref. 14 report 1.06 mas, 0.6 mas, and 4.677, respectively). Likewise, our derived separations recover the known orbit of the system (see Fig 21). We note that for the earlier portion of the night, when contemporaneous MIRC-X data were recorded, the reduced MYSTIC data show a small systematic shift in position compared to MIRC-X, implying a small wavelength miscalibration for MYSTIC. This will be corrected in future versions of the data reduction pipeline.

8.2 Future upgrades

A few avenues are still available to improve the sensitivity of the instrument in the near future, which we mention briefly mention here.

We have developed a pupil tracker, the Six Telescope Star Tracker (STST), to continuously monitor the CHARA beam drift, which will be installed at CHARA in early August, 2022. We will insert a beamsplitter into each of the CHARA IR beams, extracting 5 % of the near infrared light. This light will then be directed into an 8″ Cassegrain telescope (Orion SkyQuest XT8) with its eyepiece removed and replaced with a collimator. The compressed beams will then be tracked with a C-RED 2 camera from First Light, operating at 600 Hz, and beam drift will be corrected for by the CHARA lab-AO tip/tilt system. We anticipate a factor-of-two improvement in total photon coupling into the MYSTIC fibers once this system is operational.

We suspect that over half of the background flux measured on the detector originates from the warm sapphire window separating the MYSTIC cryostat from the camera's internal dewar. We plan to test this hypothesis by removing the window sometime early next year. We note that this option does pose some additional risk to the camera, as any rapid pressure increase in the MYSTIC dewar may cause the camera filters to shatter and damage the detector.

Finally, pending additional sources of funding for the instrument, we could replace the C-RED One camera for a newer version with a lower overall background. MIRC-X and MYSTIC feature the first two commercially produced SAPHIRA detector-based cameras, and newer units resolve some early electronic tuning and isolation issues present in our cameras. For instance, new units are electronically isolated from the camera's cryo-pump and no longer exhibit a 94 Hz nuisance oscillation in the detector readout. Optimistically, a newer detector could provide an additional three-fold improvement in sensitivity over the aforementioned upgrades.

These upgrades together could yield an upwards of 2.7 magnitude sensitivity boost in the K-band, allowing regular observations of objects as faint as 10th magnitude. Such an improvement would enable imaging of hundreds of YSO (especially T-Tauri) and asymptotic giant branch (AGB) targets.
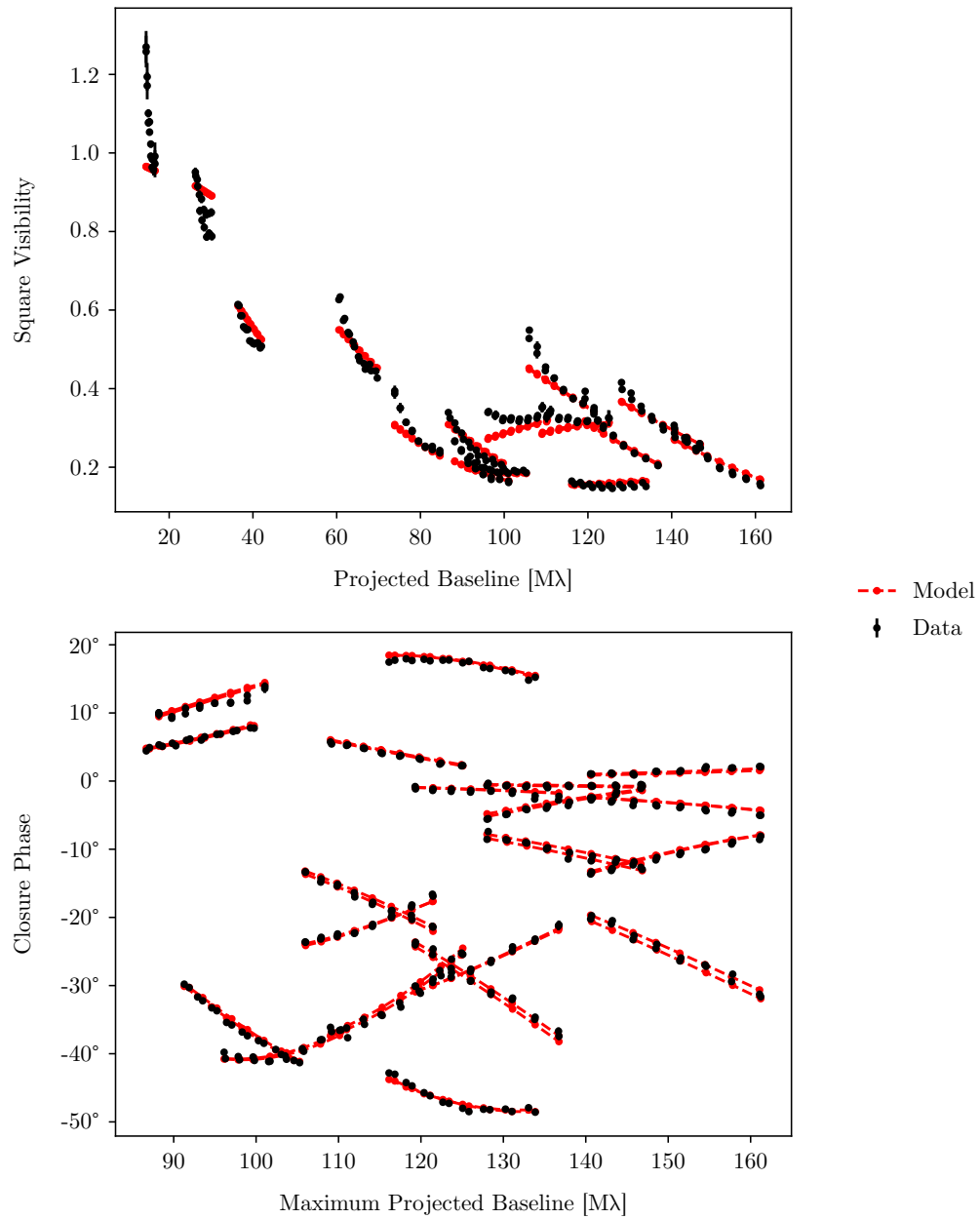
Figure 20. Sample MYSTIC data reduction and model fit to the binary star system ι Peg. Closure phases (bottom) show excellent agreement with the model binary. Square visibility measurements (top) exhibit some mis-calibration, especially at the shortest baseline, which will be addressed in future versions of the data reduction pipeline.
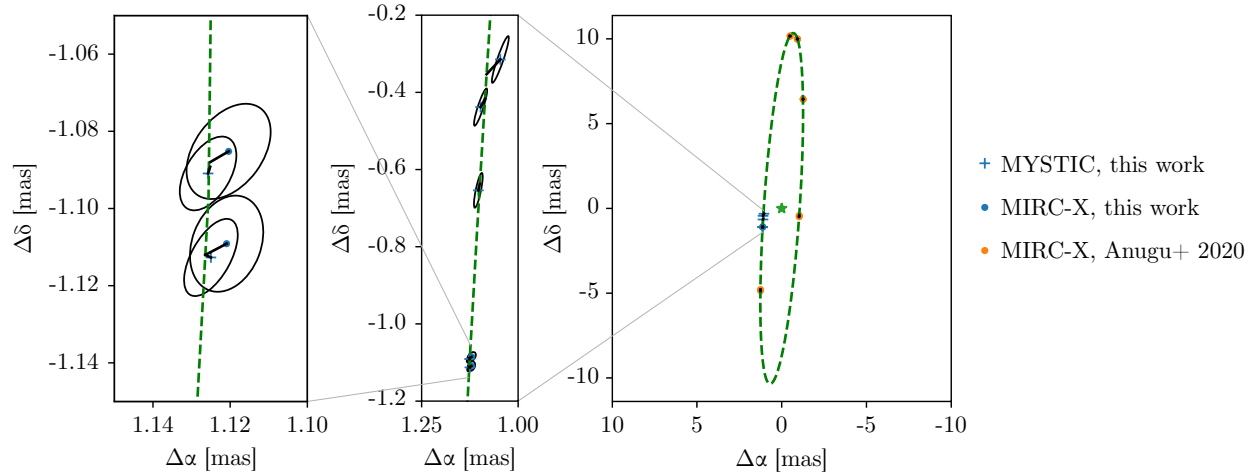
Figure 21. Fit binary separations with orbital parameters derived in Ref. 5 superimposed.

9. CONCLUDING REMARKS

MYSTIC is a science-ready instrument which meets its design goals for concurrent YSO observations with the MIRC-X combiner. Six beam solo fringe tracking has been demonstrated for objects as faint as Kmag = 7.7 at an $R = 50$ spectral resolution, and MYSTIC is able to co-track fringes with MIRC-X for observations of fainter objects.[13] We report an approximately 3 times higher thermal background than anticipated at the detector, lowering our overall sensitivity by 0.6 magnitudes, which we hope to correct with future improvements. We are in the process of optimizing the data reduction pipeline to provide data products with the required $<2\%$ for square visibility and $<0.1°$ closure phase errors.

The entire footprint of the MYSTIC instrument fits on a shared optical bench with MIRC-X. The cold optic system is installed inside of a vacuum cryostat and accommodates a six-beam image plane combiner (AIO) as well as a four-beam integrated optics combiner (ABCD). A spectrograph inside the dewar allows for spectro-interferometric observations with spectral resolutions ranging from $R = 20$ to 1724. The warm and cold optic systems are connected via commercially available single-mode, polarization-maintaining, silica fibers with good throughput performance. The cryostat is positioned so that it does not interfere with the FLUOR beams.

MYSTIC is fully motorized so that observers can operate the instrument entirely remotely. MIRC-X and MYSTIC use a shared software architecture and MYSTIC adopts nearly the same GUIs as those already familiar to users of MIRC-X; even subsystems with different hardware implementations between the two instruments, such as the fiber injection strategy, provide a uniform interface for the observer. Both instruments use a single, common GUI for data collection and high level observing tasks. A continually running server logs the vacuum status, temperature, vibration, hard drive usage, and camera status of both instruments, and an automatic system health summary is generated every 12 hours and posted to an internal Slack channel.

The optical train of MYSTIC implements a few refinements over the MIRC-X system, including an improved fiber injection system and a motorized filter wheel for fully automated operation. We hope to integrate these features into the MIRC-X beam train in the future. Progress is underway for co-phased observations with the forthcoming SPICA instrument,[15] which will extend simultaneous CHARA observations to visible wavelengths, and further improvements to MYSTIC's sensitivity are forthcoming.

ACKNOWLEDGMENTS

REFERENCES

[1] ten Brummelaar, T. A., McAlister, H. A., Ridgway, S. T., Bagnuolo, W. G., J., Turner, N. H., Sturmann, L., Sturmann, J., Berger, D. H., Ogden, C. E., Cadman, R., Hartkopf, W. I., Hopper, C. H., and Shure, M. A., "First Results from the CHARA Array. II. A Description of the Instrument," *ApJ* **628**, 453–465 (July 2005).

[2] Monnier, J. D., Pedretti, E., Thureau, N., Berger, J.-P., Millan-Gabet, R., ten Brummelaar, T., McAlister, H., Sturmann, J., Sturmann, L., Muirhead, P., Tannirkulam, A., Webster, S., and Zhao, M., "Michigan Infrared Combiner (MIRC): commissioning results at the CHARA Array," in [*Society of Photo-Optical Instrumentation Engineers (SPIE) Conference Series*], Monnier, J. D., Schöller, M., and Danchi, W. C., eds., *Society of Photo-Optical Instrumentation Engineers (SPIE) Conference Series* **6268**, 62681P (June 2006).

[3] Finger, G., Baker, I., Alvarez, D., Ives, D., Mehrgan, L., Meyer, M., Stegmeier, J., and Weller, H. J., "SAPHIRA detector for infrared wavefront sensing," in [*Adaptive Optics Systems IV*], Marchetti, E., Close, L. M., and Vran, J.-P., eds., *Society of Photo-Optical Instrumentation Engineers (SPIE) Conference Series* **9148**, 914817 (Aug. 2014).

[4] Lanthermann, C., Anugu, N., Le Bouquin, J. B., Monnier, J. D., Kraus, S., and Perraut, K., "Modeling the e-APD SAPHIRA/C-RED ONE camera at low flux level. An attempt to count photons in the near-infrared with the MIRC-X interferometric combiner," *A&A* **625**, A38 (May 2019).

[5] Anugu, N., Le Bouquin, J.-B., Monnier, J. D., Kraus, S., Setterholm, B. R., Labdon, A., Davies, C. L., Lanthermann, C., Gardner, T., Ennis, J., Johnson, K. J. C., Ten Brummelaar, T., Schaefer, G., and Sturmann, J., "MIRC-X: A Highly Sensitive Six-telescope Interferometric Imager at the CHARA Array," *AJ* **160**, 158 (Oct. 2020).

[6] Gravity Collaboration, Abuter, R., Accardo, M., Amorim, A., Anugu, N., Ávila, G., Azouaoui, N., Benisty, M., Berger, J. P., Blind, N., Bonnet, H., Bourget, P., Brandner, W., Brast, R., Buron, A., Burtscher, L., Cassaing, F., Chapron, F., Choquet, É., Clénet, Y., Collin, C., Coudé Du Foresto, V., de Wit, W., de Zeeuw, P. T., Deen, C., Delplancke-Ströbele, F., Dembet, R., Derie, F., Dexter, J., Duvert, G., Ebert, M., Eckart, A., Eisenhauer, F., Esselborn, M., Fédou, P., Finger, G., Garcia, P., Garcia Dabo, C. E., Garcia Lopez, R., Gendron, E., Genzel, R., Gillessen, S., Gonte, F., Gordo, P., Grould, M., Grözinger, U., Guieu, S., Haguenauer, P., Hans, O., Haubois, X., Haug, M., Haussmann, F., Henning, T., Hippler, S., Horrobin, M., Huber, A., Hubert, Z., Hubin, N., Hummel, C. A., Jakob, G., Janssen, A., Jochum, L., Jocou, L., Kaufer, A., Kellner, S., Kendrew, S., Kern, L., Kervella, P., Kiekebusch, M., Klein, R., Kok, Y., Kolb, J., Kulas, M., Lacour, S., Lapeyrère, V., Lazareff, B., Le Bouquin, J. B., Lèna, P., Lenzen, R., Lévêque, S., Lippa, M., Magnard, Y., Mehrgan, L., Mellein, M., Mérand, A., Moreno-Ventas, J., Moulin, T., Müller, E., Müller, F., Neumann, U., Oberti, S., Ott, T., Pallanca, L., Panduro, J., Pasquini, L., Paumard, T., Percheron, I., Perraut, K., Perrin, G., Pflüger, A., Pfuhl, O., Phan Duc, T., Plewa, P. M., Popovic, D.,

Rabien, S., Ramírez, A., Ramos, J., Rau, C., Riquelme, M., Rohloff, R. R., Rousset, G., Sanchez-Bermudez, J., Scheithauer, S., Schöller, M., Schuhler, N., Spyromilio, J., Straubmeier, C., Sturm, E., Suarez, M., Tristram, K. R. W., Ventura, N., Vincent, F., Waisberg, I., Wank, I., Weber, J., Wieprecht, E., Wiest, M., Wiezorrek, E., Wittkowski, M., Woillez, J., Wolff, B., Yazici, S., Ziegler, D., and Zins, G., "First light for GRAVITY: Phase referencing optical interferometry for the Very Large Telescope Interferometer," *A&A* **602**, A94 (June 2017).

[7] Kenyon, S. J. and Hartmann, L., "Pre-Main-Sequence Evolution in the Taurus-Auriga Molecular Cloud," *ApJS* **101**, 117 (Nov. 1995).

[8] Perraut, K., Jocou, L., Berger, J. P., Chabli, A., Cardin, V., Chamiot-Maitral, G., Delboulbé, A., Eisenhauer, F., Gambérini, Y., Gillessen, S., Guieu, S., Guerrero, J., Haug, M., Hausmann, F., Joulain, F., Kervella, P., Labeye, P., Lacour, S., Lanthermann, C., Lapras, V., Le Bouquin, J. B., Lippa, M., Magnard, Y., Moulin, T., Noël, P., Nolot, A., Patru, F., Perrin, G., Pfuhl, O., Pocas, S., Poulain, S., Scibetta, C., Stadler, E., Templier, R., Ventura, N., Vizioz, C., Amorim, A., Brandner, W., and Straubmeier, C., "Single-mode waveguides for GRAVITY. I. The cryogenic 4-telescope integrated optics beam combiner," *A&A* **614**, A70 (June 2018).

[9] Lazareff, B., Le Bouquin, J. B., and Berger, J. P., "A novel technique to control differential birefringence in optical interferometers. Demonstration on the PIONIER-VLTI instrument," *A&A* **543**, A31 (July 2012).

[10] Sturmann, L., Sturmann, J., ten Brummelaar, T., and McAlister, H. A., "Nine-channel tip/tilt detector at the CHARA Array," in [*Society of Photo-Optical Instrumentation Engineers (SPIE) Conference Series*], Monnier, J. D., Schöller, M., and Danchi, W. C., eds., *Society of Photo-Optical Instrumentation Engineers (SPIE) Conference Series* **6268**, 62683T (June 2006).

[11] Shaklan, S. B. and Roddier, F., "Single-mode fiber optics in a long-baseline interferometer," *Appl. Opt.* **26**, 2159–2163 (June 1987).

[12] Gach, J. L., Feautrier, P., Stadler, E., Greffe, T., Clop, F., Lemarchand, S., Carmignani, T., Boutolleau, D., and Baker, I., "C-RED one: ultra-high speed wavefront sensing in the infrared made possible," in [*Adaptive Optics Systems V*], Marchetti, E., Close, L. M., and Véran, J.-P., eds., *Society of Photo-Optical Instrumentation Engineers (SPIE) Conference Series* **9909**, 990913 (July 2016).

[13] Anugu, N., Monnier, J. D., Le Bouquin, J.-B., Kraus, S., Setterholm, B. R., ten Brummelaar, T. A., Schaefer, G., Lanthermann, C., and Ennis, J., "CHARA MIRC-X and MYSTIC cophasing observations to enable efficient spectro-interferometry and over-resolved object imaging," in [*Optical and Infrared Interferometry and Imaging VIII*], Mérand, A., Sallum, S., and Sanchez-Bermudez, J., eds., *Society of Photo-Optical Instrumentation Engineers (SPIE) Conference Series* **12183**, 12183–18 (July 2022).

[14] Konacki, M., Muterspaugh, M. W., Kulkarni, S. R., and Hełminiak, K. G., "High-precision Orbital and Physical Parameters of Double-lined Spectroscopic Binary Stars—HD78418, HD123999, HD160922, HD200077, and HD210027," *ApJ* **719**, 1293–1314 (Aug. 2010).

[15] Mourard, D., Berio, P., Pannetier, C., Nardetto, N., Albrecht, S., Allouche, F., Bailet, C., Bourgès, L., ten Brummelaar, Theo A.and Creevey, O., Deheuvels, S., Dejonghe, J., Domiciano, A., Geneslay, P., Gies, D. R., Jacqmart, E., Lagarde, S., Lecron, D., Ligi, R., Mella, G., Morand, F., Rousseau, S., Salabert, D., Schaefer, G., Spang, A., and Wittkowski, M., "CHARA/SPICA: a new 6T instrument for the CHARA Array," in [*Optical and Infrared Interferometry and Imaging VIII*], Mérand, A., Sallum, S., and Sanchez-Bermudez, J., eds., *Society of Photo-Optical Instrumentation Engineers (SPIE) Conference Series* **12183**, 12183–7 (July 2022).